SPYROS GKORMPATSIS

VISCOELASTIC FLOW AROUND PARTICLES USING THE OLDROYD-B AND EXP-PTT MODELS

MASTER'S THESIS

UNIVERSITY OF THE AEGEAN | DEPARTMENT OF MATHEMATICS
KARLOVASI | 27 MAY 2019

SUPERVISOR: KONSTANTINOS HOUSIADAS

EXAMINERS: KONSTANTINOS HOUSIADAS

AGAPITOS HATZINIKITAS

GEORGIOS GEORGIOU

First, I would like to thank my supervisor professor, K. D. Housiadas, for his guidance and advice he has provided throughout my time as postgraduate student and especially for his support to my work on this thesis.

I am very glad and thankful that I had the chance to meet and collaborate with professors, R. I. Tanner and A. N. Beris.

Special thanks go to my friend and colleague, E. A. Gryparis, even though we know each other for a long time he proved to be a great collaborator.

Finally, my deep and sincere gratitude to my family for their continuous help and support all these years.

CONTENTS

ABSTRACT

In fluid mechanics we have three fundamental problems for the flow around particles are pure *shear* and *elongational* flow imposed far from the particles, and *steady translation* of the particles with constant velocity. Here we study analytically an elongational flow around a cylindrical particle and a steady translation of a spherical particle. We assume the ambient fluid to be viscoelastic and modelled with Upper Convected Maxwell, Oldroyd-B (UCM) and exponential Phan-Thien and Tanner (exp-PTT) under isothermal and creeping flow conditions. The solution for all the dependent variables is expanded as an asymptotic power series with the small parameter being the Weissenberg number, Wi. The resulting sequence of equations is solved analytically up to fourth order in the Weissenberg number.

In the first chapter we study the effect of steady planar elongational flow past an infinitely long circular cylinder. Here the small parameter is the Weissenberg number which is defined as the product of the single relaxation time of the fluid "λ" times the constant rate of elongation "$\dot{\varepsilon}$", $Wi \equiv \dot{\varepsilon}\lambda$. In the second chapter we study the effect of Navier type slip on the surface of a spherical particle which translates with constant velocity U in a viscoelastic ambient fluid. Again, the small parameter here is the Weissenberg number which is defined as $Wi \equiv \lambda U/R$ where λ is the single relaxation time of the fluid and R the radius of the particle. Also, for the steady translation we applied techniques to accelerate the convergence of series solutions in order to derive more accurate expressions for the drag force on the particle.

This thesis is part of my work at [E. A. Gryparis, S. D. Gkormpatsis, K. D. Housiadas and R. I. Tanner, "Viscoelastic planar elongational flow past an infinitely long cylinder", Physics of Fluids 31, 033104, (2019)]; (see Ref. [1]) and [S. D. Gkormpatsis, E. A. Gryparis, K. D. Housiadas and A. N. Beris, "Steady sphere translation in a viscoelastic fluid with slip on the surface of the sphere", Journal of Non-Newtonian Fluid Mechanics 275, 104217, (2020)]; (see Ref. [2]).

1. VISCOELASTIC PLANAR ELONGATIONAL FLOW PAST AN INFINITELY LONG CYLINDER

1.1 INTRODUCTION

The motion of rigid particles in neutrally buoyant, non-Brownian suspensions is a very active and difficult subject, important for theoretical purposes, the development of new computational methods, as well as for the progress in industrial and real-world applications. Of great interest is the case under which the suspension is subjected to a macroscopic velocity profile such as simple steady shear, uniaxial elongation, and planar elongation. Although these situations represent oversimplification of the true flows that occurs during the processing of suspensions, the study of these flows represents the first step towards the deeper understanding of the rheological behavior of suspensions. The literature on the subject is vast; thus, the interested reader is referred to a recent review and references therein [3].

A fundamental task in the theory of suspensions is the study of the flow of the surrounding (matrix) fluid around a single particle ignoring the presence of all the other particles and under the simplest possible conditions. For a Newtonian matrix fluid and a rigid particle (usually a sphere or a circular cylinder), there are analytical Stokes-flow solutions available in the literature for both simple shear and uniaxial elongation [4].

However, when the matrix fluid has viscoelastic properties and even in absence of inertia, the situation is much more complex because the relevant governing equations, i.e. the mass and momentum balances and the constitutive model which describes the response of the matrix fluid under flow deformation, are strongly non-linear [5], [6]. As such, they cannot be solved analytically. In the case of a spherical rigid particle there are available in the literature a big variety of approximate analytical solutions as well as numerical solutions. This problem is considered nowadays as a benchmark for the development of new numerical methods [7]. In the case of a cylindrical rigid particle, the only available analytical solution is for steady shearing [8], but for elongation flow there are no solutions, either exact or approximate. Numerical solutions are also very scarce; the work by Hwang & Hulsen [9] for planar elongation of many circular particles, but in a Newtonian matrix fluid, is worth mentioning here.

The goal of the present work is to investigate how viscoelasticity affects the flow around a cylindrical particle. The latter is considered very long in order to avoid finite length effects which would lead to a three-dimensional flow field. The flow is assumed creeping, steady, and isothermal. Far from the particle, planar elongation with constant rate of elongation is imposed. No external forces and torques are applied on the particle, which in conjunction with the symmetries of the planar elongation, means that the particle does not rotate. Under these conditions, the hydrodynamic force acting on the particle is such that the resultant force and torque are zero.

Finding analytically the exact solution of the non-linear governing equations that describe this problem has been an unfeasible task so far. In order to accomplish this goal, we follow the methodology described previously by Housiadas & Tanner [8] adopting a regular perturbation scheme [10] valid for small values of the dimensionless Weissenberg number, Wi; the latter is defined as the product of the single relaxation time of the fluid times the constant rate of elongation. Thus, we are limited to small departures from the Newtonian response; however, we expect that the results will also serve as a guide for further numerical exploration of the problem. We solve the resulting sequence of equations analytically up to fourth order in Wi and we find the first five terms in the perturbation expansions. Our previous experience for the same problem under pure steady shearing showed that the high-order terms do not increase the accuracy of the solution [8].

The rest of this chapter is organized as follows. In Sec.1.2, we present the governing equations, along with the accompanying boundary conditions, in dimensionless form. In Sec.1.3, we present briefly our method of solution, and we also give the analytical solution for all the dependent primary flow variables up to 2nd order in the Weissenberg number. Last, in Sec.1.4, we present the main features of the solution, we comment on the accuracy and validity of the solution, and we discuss the most interesting results along with some conclusions.

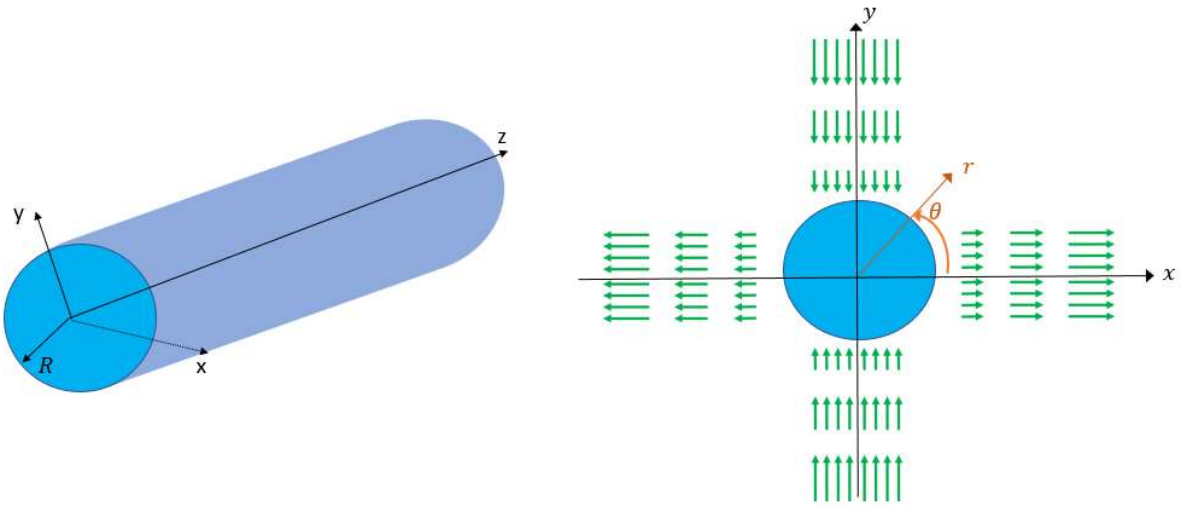

Figure (1.1): Geometrical configuration and coordinate systems.

The far flow-field planar elongational velocity is illustrated too.

1.2 GOVERNING EQUATIONS

We consider the isothermal, steady, and planar elongational flow of an incompressible viscoelastic fluid with constant mass density ρ, past an infinitely long circular cylinder with constant radius R. The domain of the ambient fluid is unbounded in order to avoid the effect of walls. Cylindrical coordinates, $r\theta z$, are used to describe the flow as well as Cartesian coordinates, xyz, for the far flow-field where the z-axis is the same in both coordinate systems; see Figure (1.1). The Cartesian coordinates are expressed in terms of the cylindrical coordinates as $x = r\cos(\theta)$, $y = r\sin(\theta)$, $z = z$. Far from the body a planar elongational velocity field is assumed, i.e. $v_x^\infty = x\,\dot{\varepsilon}$, $v_y^\infty = -y\,\dot{\varepsilon}$, $v_z^\infty = 0$where $\dot{\varepsilon}$ is the constant elongational rate; throughout the paper the superscript ∞ denotes the far flow-field (or value at infinity). The pressure at infinity is constant and can be taken to be zero, $p^\infty = 0$. The fluid is viscoelastic, consisting of a pure solvent and a polymer contribution with zero shear-rate viscosities η_s and η_p, respectively. The single relaxation time of the polymer is denoted by λ. Note that the axis of symmetry of the cylinder is aligned with the direction of vorticity which remains always perpendicular to the plane of flow, i.e. to the plane xy. The velocity vector and the total pressure are denoted by $\mathbf{v}, p$, respectively, and the viscoelastic extra-stress tensor by $\boldsymbol{\tau}$. We use R to dimensionalize all lengths, $\dot{\varepsilon}R$ for the velocity components, $(\eta_s + \eta_p)\dot{\varepsilon}$ for the pressure, and $\eta_p\,\dot{\varepsilon}$ for the viscoelastic extra-stress components. In absence of external forces and torques and neglecting inertia, the dimensionless governing equations are the mass and momentum balances. In a Eulerian frame of reference and at steady state, these equations are:

$$\nabla \cdot \mathbf{v} = 0 \tag{1.1}$$

$$-\nabla p + (1-\eta)\nabla^2 \mathbf{v} + \eta\, \nabla \cdot \boldsymbol{\tau} = \mathbf{0} \tag{1.2}$$

The extra-stress tensor $\boldsymbol{\tau}$ due to viscoelasticity is determined utilizing the following constitutive models:

$$\exp\big(\varepsilon\, Wi\ \mathrm{tr}(\boldsymbol{\tau})\big)\boldsymbol{\tau} + Wi \frac{\delta \boldsymbol{\tau}}{\delta t} = \dot{\boldsymbol{\gamma}} \tag{1.3}$$

In Eq.(1.3), $\dot{\boldsymbol{\gamma}} = \nabla \mathbf{v} + (\nabla \mathbf{v})^T$ is the rate-of-strain tensor, $\mathrm{tr}(\bullet)$ denotes the trace operator, and $\delta\boldsymbol{\tau}/\delta t$ represents the Upper Convected derivative of $\boldsymbol{\tau}$:

$$\frac{\delta \boldsymbol{\tau}}{\delta t} := \frac{\partial \boldsymbol{\tau}}{\partial t} + (\mathbf{v} \cdot \nabla)\boldsymbol{\tau} - \boldsymbol{\tau} \cdot \nabla \mathbf{v} - (\nabla \mathbf{v})^T \cdot \boldsymbol{\tau} \tag{1.4}$$

Eq.(1.3) is the exponential Phan-Thien and Tanner model (exp-PTT) and ε is the rheological parameter of the model. For more details on the constitutive models the interesting reader is referred to [11].

In Eq.(1.2) η is the dimensionless polymer viscosity ratio $\eta \equiv \eta_p/(\eta_s + \eta_p)$, and in Eq.(1.3) $Wi \equiv \dot{\varepsilon}\, \lambda$ is the Weissenberg number. For $\varepsilon = 0$ the above constitutive models reduce:

(i) to the Upper Convected Maxwell (UCM) model for $\eta = 1$,

(ii) to the Newtonian model for $\eta = 0$, and

(iii) to the Oldroyd-B model for $0 < \eta < 1$.

Instead of $\boldsymbol{\tau}$ it is easier to work with another second order and symmetric tensor $\boldsymbol{\sigma}$ which is expressed with the aid of $\boldsymbol{\tau}$ and $\dot{\boldsymbol{\gamma}}$:

$$\boldsymbol{\tau} = \dot{\boldsymbol{\gamma}} - Wi\, \boldsymbol{\sigma} \tag{1.5}$$

Substituting $\boldsymbol{\tau}$ in Eqs.(1.2)-(1.3) a new form of the equations is easily derived Ref. [8]. The domain of definition of the equations is $\{1 < r < \infty, 0 \le \theta < 2\pi\}$ and the problem is two-dimensional. Thus, in principle, the final equations are seven scalar partial differential equations in two spatial dimensions (r and θ).

The required boundary conditions are specified at $r = 1$ and at $r \to \infty$, while periodicity is imposed in the azimuthal angle θ. In particular, no-slip and no-penetration conditions in conjunction with the symmetry of the far flow-field lead to zero velocity on the surface of the cylinder:

$$\mathbf{v} = \mathbf{0} \quad \text{at} \quad r = 1 \tag{1.6}$$

Far from the body, at $r \to \infty$, the velocity approaches the velocity of the ambient fluid and the pressure becomes equal to a constant (datum) pressure which can be taken to be zero

$$\mathbf{v}^{\infty} = x\,\mathbf{e}_x - y\,\mathbf{e}_y, \quad p^{\infty} = 0 \tag{1.7}$$

In cylindrical polar coordinates, the far flow-field is expressed as $\mathbf{v}^{\infty} = r\cos(2\theta)\mathbf{e}_r - r\sin(2\theta)\mathbf{e}_\theta$. Eq.(1.7) leads to a constant rate-of-strain tensor $\dot{\boldsymbol{\gamma}}^{\infty} = 2\mathbf{e}_x\mathbf{e}_x - 2\mathbf{e}_y\mathbf{e}_y$, and a constant extra-stress tensor $\boldsymbol{\sigma}^{\infty}$ which depends on the constitutive model, i.e. $\boldsymbol{\sigma}^{\infty}$ depends only on Wi and ε, while no variations with respect to the space coordinates are predicted. Note however, that with the method of solution used here boundary conditions for $\boldsymbol{\sigma}$ are not required (and cannot be imposed). They are only used a-posteriori, after the analytical solution has been calculated, as an independent check of the correctness and accuracy of the solution.

1.3 SOLUTION METHODOLOGY

The method of solution and the solution procedure has been described in Ref. [8]. For completeness, we briefly mention that we use a regular perturbation scheme in terms of the Weissenberg number, i.e. the solution for all the dependent variables is given as a power series expansion in terms of Wi:

$$X \approx \sum_{j=0} Wi^j X_j\,, \quad X = \mathbf{v}, p, \boldsymbol{\sigma} \tag{1.8}$$

where the zero-order term, X_0, corresponds to the Newtonian fluid. Since the UCM derivative depends linearly on $\mathbf{v}$ and $\nabla\mathbf{v}$, it is also expanded as follows:

$$\begin{gathered} \frac{\delta(\bullet)}{\delta t} = \sum_{j=0} Wi^j \frac{\delta_j(\bullet)}{\delta t}, \\ \frac{\delta_j(\bullet)}{\delta t} := \mathbf{v}_j \cdot \nabla(\bullet) - (\bullet)\cdot\nabla\mathbf{v}_j - \left(\nabla\mathbf{v}_j\right)^T \cdot (\bullet) \end{gathered} \tag{1.9}$$

Where $\partial/\partial t = 0$ has been considered. Expressions (1.8) and (1.9) are substituted in the governing equations and a sequence of equations at $O\left(Wi^j\right)$, $j = 0,1,2,\ldots$ results. By introducing $\boldsymbol{\sigma}_{-1} = \mathbf{0}$ for completeness, these equations are:

$$\nabla \cdot \mathbf{v}_j = 0 \tag{1.10}$$

$$-\nabla p_j + \nabla^2 \mathbf{v}_j = \eta \nabla \cdot \boldsymbol{\sigma}_{j-1} \tag{1.11}$$

$$\nabla^2 p_j + \eta \nabla \cdot \left(\nabla \cdot \boldsymbol{\sigma}_{j-1}\right) = 0 \tag{1.12}$$

where the boundary conditions at any order $j > 0$ are homogenous, i.e. $\mathbf{v}_j(r=1) = \mathbf{v}_j^{\infty} = \mathbf{0},\ \partial v_{r,j}/\partial r\big|_{r=1} = p_j^{\infty} = 0$. Eq. (1.12) is derived by taking the divergence of Eq. (1.11) in conjunction with the continuity equation Eq. (1.10). It is not an independent equation but is used only because it facilitates the solution procedure. Notice that Eqs. (1.10)-(1.12) contain only two unknowns, $\mathbf{v}_j$ and p_j, since the auxiliary extra-stress tensor $\boldsymbol{\sigma}_{j-1}$ is found from the constitutive model, Eq. (1.3), in terms of the solution at the previous orders in Wi. For $j = 0$ Eqs. (1.10)-(1.12) correspond to the simple Newtonian fluid, the solution of which in cylindrical coordinates and components is:

$$\begin{aligned} p_0 &= -\frac{4}{r^2}\cos(2\theta), \\ v_{r,0} &= \left(\frac{1}{r^3} - \frac{2}{r} + r\right)\cos(2\theta), \\ v_{\theta,0} &= \left(\frac{1}{r^3} - r\right)\sin(2\theta). \end{aligned} \tag{1.13}$$

It can be trivially confirmed that Eqs. (1.13) satisfies the far flow-field conditions, the zero velocity on the surface of the cylinder, as well as $\partial v_{r,0}/\partial r = 0$ at $r = 1$. The latter is a consequence of the no-slip and no-penetration of the fluid on the cylinder along with the continuity equation evaluated at $r = 1$.

By solving sequentially Eqs. (1.10)-(1.12) for $j = 0,1,2,\ldots$ and 4 we derive the solution analytically up to $O(Wi^4)$. At orders higher than two, this task is achieved by developing a symbolic code with the "Mathematica" software [12] with the aid of which the solution is also checked for its correctness. We also mention that the solution is found up to 4th-order because as verified for simple shearing in [8], the higher order terms seem to diverge.

The first-order solution is given as:

$$\begin{aligned} p_1 &= 2\eta\left\{\frac{8}{r^4} + \frac{9}{r^8} - \frac{16}{r^6} - \frac{2}{r^4}\cos(4\theta)\right\}, \\ v_{r,1} &= \ v_{\theta,1} = 0 \end{aligned} \tag{1.14}$$

Eq.(1.14) shows that the first-order correction to the velocity field due to viscoelasticity is zero while for the pressure is not, a feature which has also been predicted for the simple shearing case [8]. It is also interesting that the rheological parameter ε for the exp-PTT model, do not enter in the solution.

At 2nd order, the solution for the UCM ($\eta = 1$) and Oldroyd-B ($0 < \eta < 1$) models is:

$$
\begin{aligned}
p_2 &= \eta \left\{ \begin{array}{c} \left(\frac{864}{7r^{12}} - \frac{540}{r^{10}} + \frac{4224}{5r^8} - \frac{564}{r^6} + \frac{144}{r^4} - \frac{736}{35r^2}\right)\cos(2\theta) \\ + \left(-\frac{48}{5r^4} + \frac{4}{r^6}\right)\cos(6\theta) \end{array} \right\} \\
v_{r,2} &= \eta \left\{ \begin{array}{c} \left(-\frac{3}{7r^{11}} + \frac{26}{5r^9} - \frac{106}{5r^7} + \frac{50}{r^5} - \frac{1087}{35r^3} - \frac{88}{35r} + \frac{48\ln(r)}{r^3}\right)\cos(2\theta) \\ + \left(\frac{9}{5r^7} - \frac{18}{5r^5} + \frac{9}{5r^3}\right)\cos(6\theta) \end{array} \right\} \\
v_{\theta,2} &= \eta \left\{ \begin{array}{c} \left(-\frac{15}{7r^{11}} + \frac{104}{5r^9} - \frac{318}{5r^7} + \frac{100}{r^5} - \frac{1927}{35r^3} + \frac{48\ln(r)}{r^3}\right)\sin(2\theta) \\ + \left(\frac{9}{5r^7} - \frac{12}{5r^5} + \frac{3}{5r^3}\right)\sin(6\theta) \end{array} \right\}
\end{aligned}
\tag{1.15}
$$

The 2nd-order solution for exp-PTT model are provided in the Appendix A with the help of Eq. (1.15), while the higher order solutions are too long to be given here.

Based on the perturbation scheme, one finds that $\boldsymbol{\tau}_j = \dot{\boldsymbol{\gamma}}_j - \boldsymbol{\sigma}_{j-1}, j = 0,1,2,3, \ldots$ where, as mentioned before, $\boldsymbol{\sigma}_{-1} = \mathbf{0}$, and the non-trivial components of the rate-of-strain tensor are given, at any order in the Weissenberg number, as $\dot{\gamma}_{rr,j} = 2\left(\partial v_{r,j}/\partial r\right)$, $\dot{\gamma}_{r\theta,j} = r^{-1}\left(\partial v_{r,j}/\partial\theta\right) + \left(\partial v_{\theta,j}/\partial r\right) - v_{\theta,j}/r$ and $\dot{\gamma}_{\theta\theta,j} = 2r^{-1}\left(\partial v_{\theta,j}/\partial\theta + v_{r,j}\right)$.

NON-PRIMARY FLOW VARIABLES

Due to the fact that the flow is two-dimensional, a stream function $\Psi = \Psi(r,\theta)$ can be defined such as $v_r = r^{-1}(\partial\Psi/\partial\theta)$ and $v_\theta = -(\partial\Psi/\partial r)$. Integrating the later and using $\Psi(1,\theta) = 0$ gives $\Psi(r,\theta) = -\int_1^r v_\theta(s,\theta)\, ds$. Using the analytical solution for v_θ, we find Ψ_0, Ψ_1 and Ψ_2 as follows:

$$
\begin{aligned}
\Psi_0 &= \left(\frac{r^2}{2} - 1 + \frac{1}{2r^2}\right)\sin(2\theta) \\
\Psi_1 &= 0 \\
\Psi_2 &= \eta \left\{ \begin{array}{c} \left(-\frac{44}{35} - \frac{1087}{70r^2} + \frac{25}{r^4} - \frac{53}{5r^6} + \frac{13}{5r^8} - \frac{3}{14r^{10}} + \frac{24\ln(r)}{r^2}\right)\sin(2\theta) \\ + \frac{3}{5r^2}\left(\frac{1}{2} - \frac{1}{r^2} + \frac{1}{2r^4}\right)\sin(6\theta) \end{array} \right\}
\end{aligned}
\tag{1.16}
$$

The stream function Ψ is also closely related to the non-trivial component of the vorticity vector $\boldsymbol{\omega} \equiv \nabla \times \mathbf{v}$, which for this type of flow is $\omega_z = -\nabla^2\Psi$. We find:

$$\omega_{z,0} = -\frac{4}{r^2}\sin(2\theta)$$

$$\omega_{z,1} = 0 \tag{1.17}$$

$$\omega_{z,2} = \eta\left\{\left(\frac{144}{7r^{12}} - \frac{156}{r^{10}} + \frac{1696}{5r^8} - \frac{300}{r^6} + \frac{96}{r^4} - \frac{176}{35r^2}\right)\sin(2\theta) + \left(\frac{48}{5r^4} - \frac{12}{r^6}\right)\sin(6\theta)\right\}$$

Last, we report the conformation tensor $\mathbf{c}$, which represents the average of all possible configurations that the polymer molecules can have in space due to the flow deformation. In dimensionless form $\mathbf{c}$ and $\boldsymbol{\tau}$ are connected as $\boldsymbol{\tau} = (\mathbf{c} - \mathbf{I})/Wi$ for the UCM, Oldroyd-B and exp-PTT models. The expressions between $\boldsymbol{\tau}$ and $\mathbf{c}$ combined with $\boldsymbol{\tau} = \dot{\boldsymbol{\gamma}} - Wi\,\boldsymbol{\sigma}$, $\mathrm{tr}(\dot{\boldsymbol{\gamma}}) = 0$ and $\mathrm{tr}(\mathbf{I}) = 3$, give:

$$\begin{aligned} \mathbf{c} &= \mathbf{I} + Wi\,\dot{\boldsymbol{\gamma}} - Wi^2\boldsymbol{\sigma} \\ \mathrm{tr}(\mathbf{c}) &= 3 - Wi^2\mathrm{tr}(\boldsymbol{\sigma}) \end{aligned} \tag{1.18}$$

for the UCM, Oldroyd-B and exp-PTT models. An important feature of the (real and symmetric second-order) conformation tensor is that it is positive definite. This implies that all its eigenvalues, and consequently its trace which equals the sum of the eigenvalues, are strictly positive, a property which is necessary for the results to have physical meaning [13]. Thus, it can be used to check the validity of an approximate solution (for more comments see Ref. [8]). For a two-dimensional and axisymmetric flow field expressed in cylindrical coordinates we have $c_{\theta z} = c_{rz} = 0$, $c_{zz} = 1$, while necessary conditions for positive definiteness are $c_{rr} > 0$, $c_{\theta\theta} > 0$ and $c_{rr}c_{\theta\theta} - c_{r\theta}^2 > 0$ Ref. [8]. We focus however on the trace of the conformation tensor and use it as a guidance of the validity of the velocity/pressure field. Following Eqs. (1.18) and using the perturbation scheme, gives a general series expansion valid for all models:

$$\mathrm{tr}(\mathbf{c}) \approx 3 - Wi^2\{\mathrm{tr}(\boldsymbol{\sigma}_0) + \mathrm{tr}(\boldsymbol{\sigma}_1)Wi + \mathrm{tr}(\boldsymbol{\sigma}_2)Wi^2 + \ldots\} \tag{1.19}$$

It is worth mentioning that at any order in Weissenberg number, the conformation tensor and its trace can be calculated up to two orders of magnitude higher than the velocity and pressure fields. For instance, when only the solution $\mathbf{v}_0$ for the Newtonian fluid is known, the trace of conformation tensor can be calculated up to second-order, namely $\mathrm{tr}(\mathbf{c}) \approx 3 - Wi^2\,\mathrm{tr}(\boldsymbol{\sigma}_0)$ since $\boldsymbol{\sigma}_0 = \boldsymbol{\sigma}_0(\mathbf{v}_0)$. Thus, in Eq. (1.19) the $O(Wi^2)$ term results exclusively from the Newtonian solution, and the $O(Wi^3)$ term from both $\boldsymbol{\sigma}_0 = \boldsymbol{\sigma}_0(\mathbf{v}_0)$ and $\boldsymbol{\sigma}_0 = \boldsymbol{\sigma}_0(\mathbf{v}_0, \mathbf{v}_1)$ For $\mathrm{tr}(\boldsymbol{\sigma}_0)$ and $\mathrm{tr}(\boldsymbol{\sigma}_1)$ we find:

$$\begin{aligned} \mathrm{tr}(\mathbf{c}) &\approx 3 - Wi^2\{\mathrm{tr}(\boldsymbol{\sigma}_0) + \mathrm{tr}(\boldsymbol{\sigma}_1)Wi + \mathrm{tr}(\boldsymbol{\sigma}_2)Wi^2 + \cdots\} \\ \mathrm{tr}(\boldsymbol{\sigma}_1) &= \left\{\begin{array}{c}\left(\frac{48}{r^2} - \frac{96}{r^4} + \frac{816}{r^6} - \frac{2496}{r^8} + \frac{2592}{r^{10}} - \frac{864}{r^{12}}\right)\cos(2\theta) \\ + \left(-\frac{240}{r^6} + \frac{384}{r^4} - \frac{144}{r^2}\right)\cos(6\theta)\end{array}\right\} \end{aligned} \tag{1.20}$$

Note that the rheological parameter ε enters for the first time in $\mathrm{tr}(\boldsymbol{\sigma}_2)$. Thus, and based on Eq. (1.19), ε affect the solution for $\mathrm{tr}(\mathbf{c})$ at $O(Wi^4)$. For the UCM, Oldroyd-B models one must set $\varepsilon = 0$ in Eqs (1.19)-(1.20) and for the exp-PTT model $\varepsilon > 0$.

1.4 RESULTS, DISCUSSION AND CONCLUSIONS

Before presenting the results, we mention briefly the following features of the asymptotic solution, all of which had also been observed for the simple shear flow Ref. [8]. First, the $O(Wi)$ correction term to the velocity field is zero, while the corresponding correction to the pressure is non-zero (see Eq. (1.14)). Thus, viscoelasticity affects the solution for the velocity vector, rate-of-strain tensor, stream function, and vorticity at second-order in the Weissenberg number.

Second, at second- and higher-orders, terms of the form $[\ln(r)]^m/r^k$, where k and m are non-negative integers, appear in the solution. These terms become maximum at a distance $r_c = \exp(m/k) \approx 1 + (m/k)$; the latter is a very approximation of the exponential term because m is small and k is large. For $m = 0$ the maximum is located on the surface of the cylinder (i.e. $r_c = 1$) but for $m > 0$ the maximum is observed farther from the body. Thus, complicated flow structures are developed near the cylinder.

Third, the analytical solution shows that only even Fourier modes contribute to the solution at any order in Weissenberg number. When only cosine modes are present the corresponding flow variable (for instance, $p, v_r, \mathrm{tr}(\boldsymbol{\sigma})$) is fully symmetric with respect to both the x- and the y-axis and up-and-down and fore-and-aft symmetries are observed, respectively (recall that $\cos(\theta) = x/\sqrt{x^2+y^2}$ and $\sin(\theta) = y/\sqrt{x^2+y^2}$). However, when sine modes appear in the solution (for instance, in Ψ, ω_z, v_θ) both symmetries break. Thus, it appears that the effect of viscoelasticity destroys the symmetries observed for a Newtonian fluid.

The correctness of our analytical solution is checked with the aid of the "Mathematica" software Ref. [12] by performing two tests. The first test is based on the governing equations Eq. (1.10)-(1.12) which, at any order in Weissenberg number $O(Wi^j)$, consist of four scalar partial differential equations with three unknowns, $v_{r,j}, v_{\theta,j}$ and p_j. According to the solution procedure, p_j is determined solving Eq. (1.12), $v_{\theta,j}$ is found in terms of $v_{r,j}$ solving Eq. (1.10), and $v_{r,j}$ is found solving the radial component of Eq. (1.11). Thus, substituting the solution for all variables in the azimuthal component of the momentum balance, Eq. (1.11), provides an independent test of its correctness.

The second test, which is also used as a guidance of the accuracy of the asymptotic solution, is based on the far flow-field viscoelastic extra-stress tensor $\boldsymbol{\sigma}^\infty$ which is calculated simply by substituting $\mathbf{v}^\infty$ in the constitutive model(s) and solving the resulting equations. Then, $\boldsymbol{\sigma}^\infty$ can be expanded and found in series form as $\boldsymbol{\sigma}^\infty = \sum_{j=0} \boldsymbol{\sigma}_j^\infty Wi^j$. However, due to the method of solution used here, $\boldsymbol{\sigma}_j^\infty$ cannot be imposed because at any order in Wi $\boldsymbol{\sigma}_j$ is fully determined using all the lower-order solutions (i.e. $\mathbf{v}_0, \mathbf{v}_1, \ldots, \mathbf{v}_{j-1}$) and the constitutive model(s) without the need to solve any differential equations (see Ref. [8] for more details). Comparing $\boldsymbol{\sigma}_j(r \to \infty)$ with $\boldsymbol{\sigma}_j^\infty$ gives another undeniable test of the correctness of the analytical solution at any order in the Weissenberg number. Furthermore, the difference between the analytical solution at infinity, $\boldsymbol{\sigma}(r \to \infty) \approx \sum_{j=0}^{4} \boldsymbol{\sigma}_j(r \to \infty) Wi^j$, and the exact solution, i.e. the quantity $\|\boldsymbol{\sigma}^\infty - \boldsymbol{\sigma}(r \to \infty)\|$ where $\|\bullet\|$ is either the Euclidian or the Frobenius norm, gives an estimate of the error of the results.

The validity of the high-order series solution which is composed by adding all the available correction terms in the Newtonian solution is another, much more difficult, issue that must be examined. Here this issue is determined mainly based on the sign of the trace of the conformation tensor. In Figure (1.2), we fix the Weissenberg number ($Wi = 1.0$) and the polymer viscosity ratio ($\eta = 1$) and look for regions with $\mathrm{tr}(\mathbf{c}) < 0$. We calculate the solution up to $\mathrm{O}(Wi^j)$ where $j = 2,3,4,5$ and 6. For $j = 2$ and 3 no regions with negative trace were found; recall that $j = 2$ corresponds to the Newtonian solution for $\mathbf{v}$ and p, while $j = 3$ corresponds to both the Newtonian and the first-order solutions for $\mathbf{v}$ and p. However, when the higher-order solutions are considered in the solution, regions with negative terms appear around the cylinder. These regions increase in number and become larger as j increases. If the Weissenberg number is decreased the regions of negative trace shrink, while the opposite trend holds when the Weissenberg number increases. All these observations are consistent with the fact that as the small parameter of the perturbation scheme increases, the solution gradually loses its accuracy and validity. Note that in the following we present results for Wi number and rheological parameters such as the conformation tensor is everywhere (or almost everywhere) positive definite.

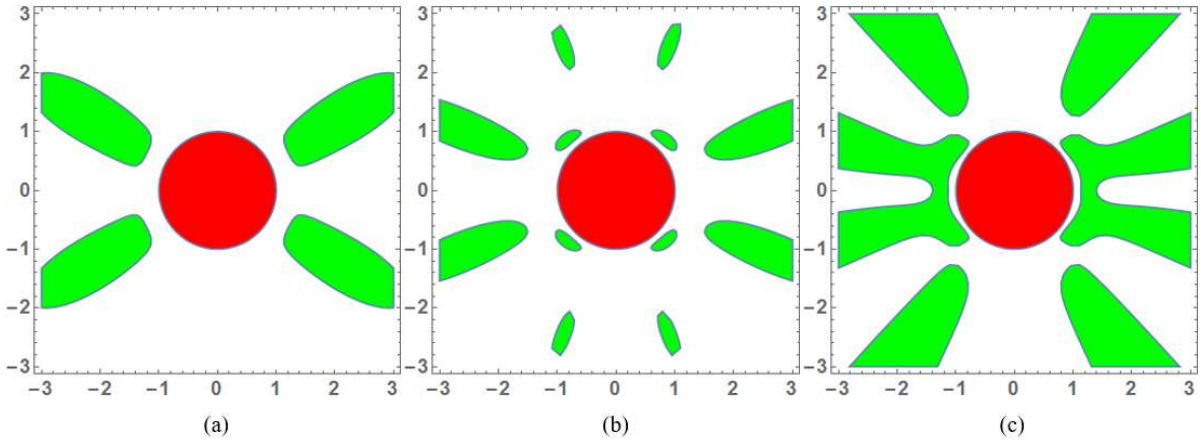

Figure (1.2): The regions of $\mathrm{tr}(\boldsymbol{c}) < 0$ (with green color) for $Wi = 1.0$ (UCM model: $\eta = 1$, $\varepsilon = 0$). The solution is calculated up to: (a) $O(Wi^4)$, (b) $O(Wi^5)$, (c) $O(Wi^6)$. The solutions up to 2nd and 3rd-orders do not show regions with negative trace.

RESULTS

Because the velocity field far from the cylinder increases linearly with the distance from the cylinder, as Eq. (1.7) shows, and the first correction term to the velocity field is $O(Wi^2)$ and varies proportionally to the powers of $1/r$, the effect of viscoelasticity on the results cannot be easily seen. In order to make the differences clear, contour plots of the stream function and vorticity are presented first for the Newtonian case, i.e. for Ψ_0 and $\omega_{z,0}$, and then for the normalized quantities:

$$\Delta\Psi_n \equiv \frac{\Psi - \Psi_0}{Wi^2} \approx \Psi_2 + Wi\,\Psi_3 + Wi^2\,\Psi_4$$
$$\Delta\omega_n \equiv \frac{\omega_z - \omega_{z,0}}{Wi^2} \approx \omega_{z,2} + Wi\,\omega_{z,3} + Wi^2\,\omega_{z,4} \qquad (1.21)$$

$$\Delta \mathrm{tr}(\mathbf{c})_n \equiv -\frac{\mathrm{tr}(\mathbf{c})-3}{Wi^2} \approx \mathrm{tr}(\boldsymbol{\sigma}_0) + \mathrm{tr}(\boldsymbol{\sigma}_1)Wi + \mathrm{tr}(\boldsymbol{\sigma}_2)Wi^2 + \cdots$$

Note that similar expressions for the pressure and the velocity, $\Delta p_n \equiv (p-p_0)/Wi$ and $\Delta \mathbf{v}_n \equiv (\mathbf{v}-\mathbf{v}_0)/Wi^2$, respectively, can also be derived. It should be emphasized here that for $Wi \to 0$, Eq. (1.21) shows that $\Delta\Psi_n$, $\Delta\omega_n$ and $\Delta \mathrm{tr}(\mathbf{c})_n$ are finite and equal to Ψ_2, $\omega_{z,2}$ and $\mathrm{tr}(\boldsymbol{\sigma}_0)$, respectively, revealing the effect of weak viscoelasticity, while the higher-order terms in Eq. (1.21) provide suitable corrections for small but finite values of Wi. Therefore, Ψ_2, $\omega_{z,2}$ and $\boldsymbol{\sigma}_0$, represent the first departure from the Newtonian fluid and they should be considered very accurate in the case of a vanishing Weissenberg number.

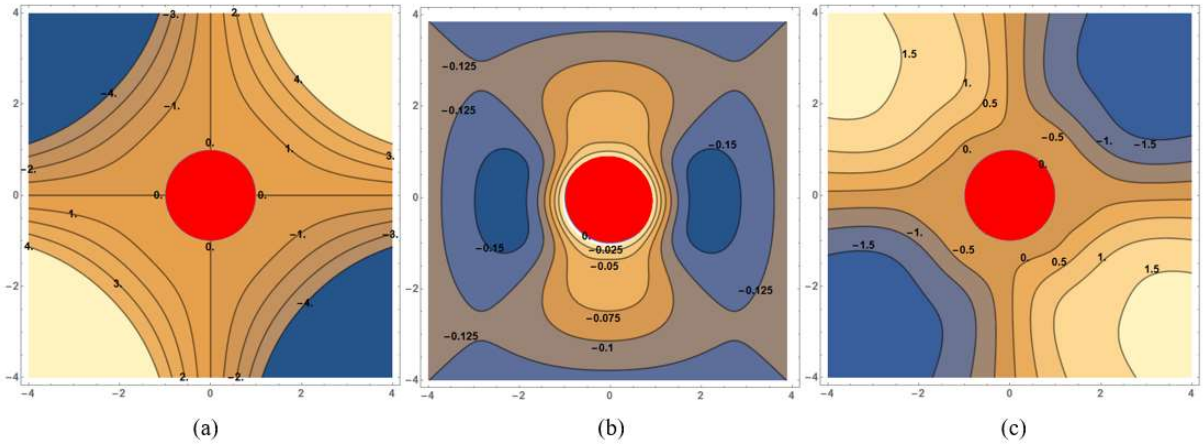

Figure (1.3): (a) Streamline contours for the Newtonian fluid ($Wi = 0$)
(b) $(\Psi - \Psi_0)/Wi^2$ as $Wi \to 0$ for a UCM fluid ($\eta = 1$, $\varepsilon = 0$)
(c) $(\Psi - \Psi_0)/Wi^2$ for a UCM fluid with $Wi = 0.5$ ($\eta = 1$, $\varepsilon = 0$)

It is known that for planar elongational flow, the streamlines for a Newtonian matrix fluid ($Wi = 0$) around a circular cylinder are open. This is seen in Figure (1.3a), in which contours for Ψ_0 are plotted; the contours values are from -4 to 4 in increments 1 (on the surface of the cylinder the stream function is zero). The up-and-down symmetry (i.e. symmetry with respect to the x-axis) as well as the fore-and-aft symmetry (symmetry with respect to the y-axis) are clearly demonstrated. For the viscoelastic case, the contours remain open too. The normalized stream function difference for $Wi \to 0$, i.e. $\Delta\Psi_n(Wi = 0) = \Psi_2$ is shown in Figure (1.3b). It is interesting that only negative values are observed which means that weak viscoelasticity reduces the flow rate compared to the Newtonian fluid. However, a different situation arises for finite Weissenberg number, as shown in Figure (1.3c) for a UCM fluid ($\eta = 1, Wi = 0.5$). On the first $(x, y > 0)$ $O(Wi^2)$ and third $(x, y < 0)$ quarters $\Delta\Psi_n$ increases substantially in magnitude, while on the second $(x < 0, y > 0)$ and the fourth $(x > 0, y < 0)$ quarters it becomes positive. In addition to that, zero contours clearly appear marking the transition from positive to negative values.

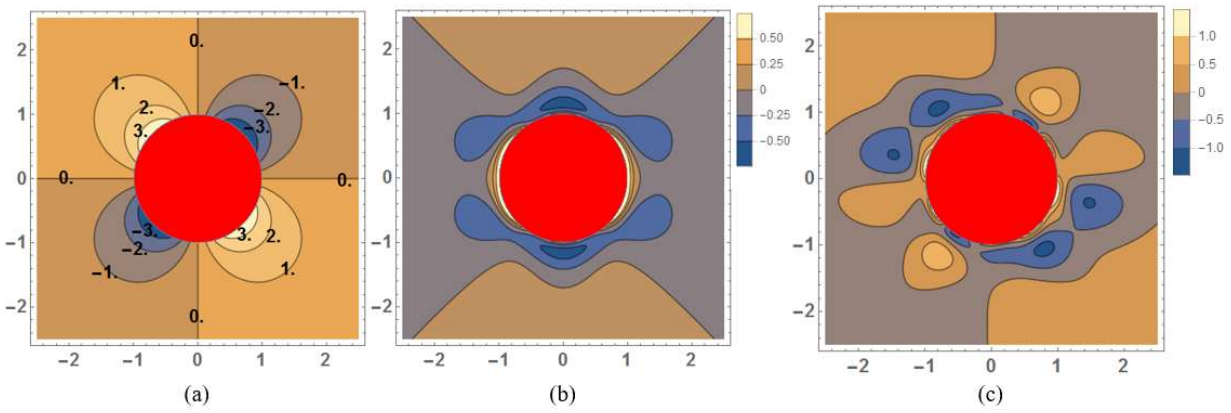

Figure (1.4): (a) Vorticity contours for the Newtonian fluid ($Wi = 0$)
(b) $(\omega_z - \omega_{z,0})/Wi^2$ as $Wi \to 0$ for a UCM fluid ($\eta = 1, \varepsilon = 0$)
(c) $(\omega_z - \omega_{z,0})/Wi^2$ for a UCM fluid with $Wi = 0.2$ ($\eta = 1, \varepsilon = 0$)

In Figure (1.4), we present contours related to the vorticity ω_z. The contours for a Newtonian fluid are shown in Figure (1.4a) from -3 to 3 in increments 1; the symmetries seen previously before for the stream function are seen here too. Moreover, contours for $\Delta\omega_n$ are given in Figures (1.4b)-(1.4c), for $Wi \to 0$ and $Wi = 0.5$, respectively. In both figures, the contour values vary from -0.075 to 0.075 in increments 0.025. When $Wi \to 0$ the vortex structures are clear (due to the second and sixth sine Fourier in the solution). However, when the higher-order corrections are included in the solution, as in Figure (1.4c), a different situation arises for finite Weissenberg number, as shown in Figure (1.4c) for a UCM fluid ($\eta = 1, Wi = 0.2$). On the first $(x, y > 0)$ $O(Wi^2)$ and third $(x, y < 0)$ quarters $\Delta\omega_n$ increases substantially, while on second $(x < 0, y > 0)$ and the fourth $(x > 0, y < 0)$ it becomes positive. In addition to that, zero contours clearly appear marking the transition from positive to negative values.

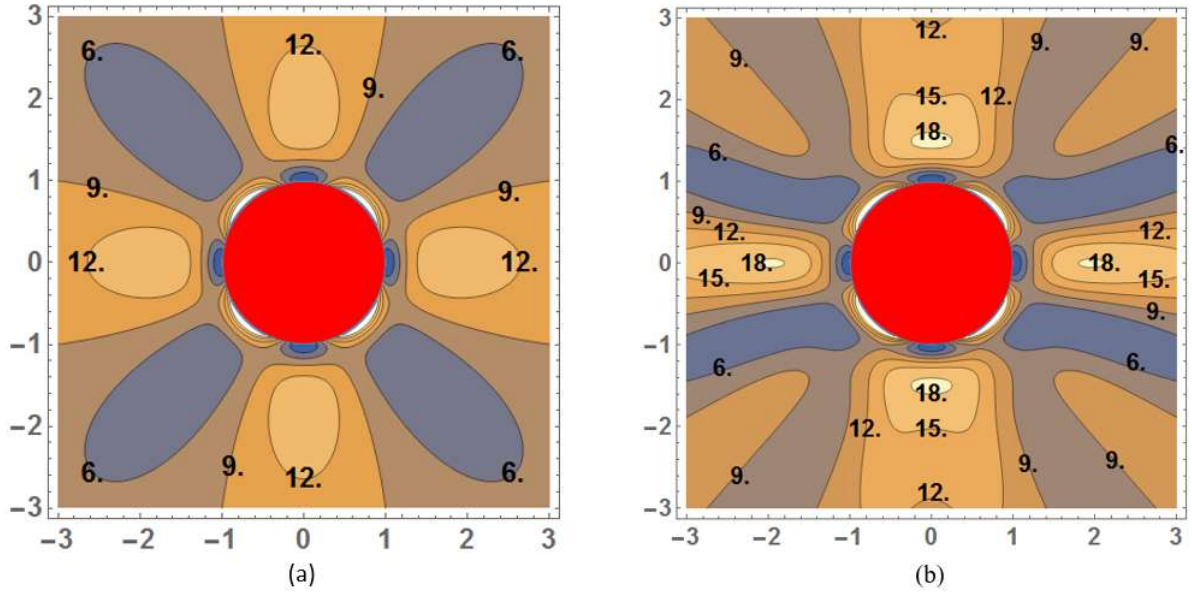

Figure (1.5): $(\mathrm{tr}(\boldsymbol{c}) - 3)/Wi^2$ contours for the UCM model ($\eta = 1, \varepsilon = 0$) (a) $Wi \to 0$ (b) $Wi = 0.2$

In Figure (1.5), we present the contours for $\Delta\mathrm{tr}(\mathbf{c})_n$ which corresponds to the extension of the polymer molecules from equilibrium. $\Delta\mathrm{tr}(\mathbf{c})_n$ is also proportional to the elastic energy stored in the polymeric molecules. The results for the Newtonian case are trivial because in this case $\mathbf{c} = \mathbf{I}$. As $Wi \to 0$ the normalized trace of the conformation tensor forms the fore-and-aft and up-and-down symmetric structures shown in Figure (1.5a), while the effect of a small but finite Weissenberg number ($Wi = 0.2$) for a UCM model is illustrated in Figure (1.5b). The substantial extension of the polymer molecules due to the strong nature of the elongational flow is seen; large contour values for $\Delta\mathrm{tr}(\mathbf{c})_n$are observed in both cases, with even larger polymer extensions that are predicted for $Wi = 0.2$.

We also present results for the dimensionless planar elongational viscosity of the fluid, $\eta_{el,p} \equiv T_{xx} - T_{yy}$ where T_{xx} and T_{yy} are components of the total stress tensor $\mathbf{T} = -p\,\mathbf{I} + (1-\eta)\dot{\boldsymbol{\gamma}} + \eta\,\boldsymbol{\tau}$. Substituting $\boldsymbol{\tau}$ with the aid of Eq. (1.5) gives $\mathbf{T} = -p\,\mathbf{I} + \dot{\boldsymbol{\gamma}} - \eta\,Wi\,\boldsymbol{\sigma}$ Thus, the final expression for $\eta_{el,p}$ is:

$$\eta_{el,p} = (\dot{\gamma}_{xx} - \dot{\gamma}_{yy}) - \eta\,Wi\,(\sigma_{xx} - \sigma_{yy}) \tag{1.22}$$

Far from the cylinder Eq.(1.22) becomes $\eta^{\infty}_{el,p} = (\dot{\gamma}^{\infty}_{xx} - \dot{\gamma}^{\infty}_{yy}) - \eta\,Wi\,(\sigma^{\infty}_{xx} - \sigma^{\infty}_{yy}) \Rightarrow \eta^{\infty}_{el,p} = 4 - \eta\,Wi\,(\sigma^{\infty}_{xx} - \sigma^{\infty}_{yy})$. The latter, for a Newtonian fluid, gives the well-known result $\eta^{\infty}_{el,p} = 4$. In general, however, the planar elongational viscosity depends on σ^{∞}_{xx} and σ^{∞}_{yy}, i.e. on the constitutive model that is used. For instance, for the UCM and Oldroyd-B models one finds:

$$\eta^{\infty}_{el,p} = 4\left(1 + \eta\,\frac{(2Wi)^2}{1-(2Wi)^2}\right) \tag{1.23}$$

Eq. (1.23) shows the increase of $\eta^{\infty}_{el,p}$ with the increase of Wi. Notice that for $Wi = 1/2$ the elongational viscosity diverges to infinity, a problem which is rectified with the use of other non-linear constitutive equations such as the exp-PTT model. Similar expression as Eq. (1.23) have been calculated for the exp-PTT model. The perturbation series expansion of Eq. (1.23) up to $O(Wi^4)$ is:

$$\eta^{\infty}_{el,p} \approx 4(1 + 4\,\eta\,Wi^2 + 16\,\eta\,Wi^4) \tag{1.24}$$

Eq. (1.24) is a very good approximation of Eq. (1.23) up to $Wi \approx 0.3$, approximately, for which a 50% increase of the elongational viscosity is predicted.

Finally, using the perturbation solution, Eq. (1.22) gives for the UCM/Oldroyd-B models:

$$\frac{\eta_{el,p}}{4} \approx 1 + \left(\frac{2}{r^2} - \frac{3}{r^4}\right)\cos(4\theta) + \begin{Bmatrix}\left(-\frac{2}{r^2} + \frac{12}{r^6} - \frac{12}{r^8}\right)\cos(2\theta) \\ +\left(\frac{6}{r^2} - \frac{20}{r^4} + \frac{16}{r^6}\right)\cos(6\theta)\end{Bmatrix}\eta\,Wi + \eta_{el,p2}\,\eta\,Wi^2 \tag{1.25}$$

where the 2nd-order correction term is given as:

$$\eta_{el,p2} = \left\{ \begin{array}{c} \left(4 - \frac{450}{7r^{12}} + \frac{756}{5r^{10}} - \frac{378}{5r^{8}} - \frac{26}{r^{6}} + \frac{12}{r^{4}}\right) \\ + \left(-\frac{135}{r^{12}} + \frac{378}{r^{10}} - \frac{252}{r^{8}} - \frac{156}{r^{6}} + \frac{5382}{35r^{4}} + \frac{368}{35r^{2}} - \frac{144\ln(r)}{r^{4}}\right)\cos(4\theta) \\ + \left(-\frac{423}{5r^{8}} + \frac{174}{r^{6}} - \frac{114}{r^{4}} + \frac{24}{r^{2}}\right)\cos(8\theta) \end{array} \right\} \qquad (1.26)$$

Taking the limit of Eq. (1.25) and (1.26) as r goes to infinity gives the first two terms of Eq. (1.24) (as it should). We also observe, by comparing Eqs. (1.24) and (1.25), that although only the even powers of the Weissenberg number contribute to the far flow-field planar elongational viscosity $\eta^{\infty}_{el,p}$, this is not the case for the local viscosity $\eta_{el,p}$ for which all the powers of Weissenberg are non-zero. This feature holds for all the constitutive models used in this work.

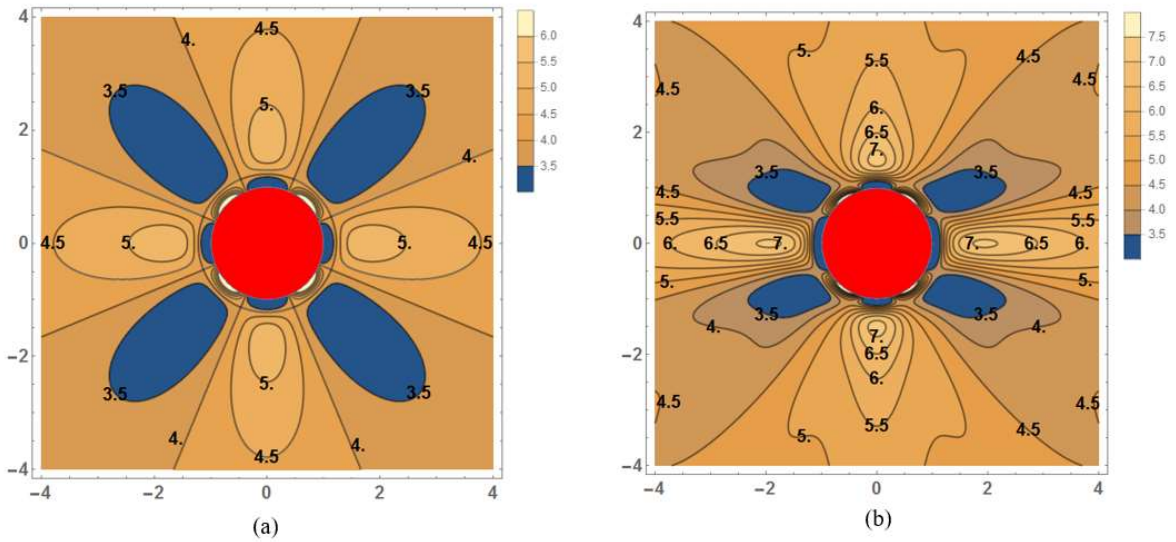

Figure (1.6): $\eta_{el,p}$ contours (a) Newtonian fluid, (b) UCM model ($\eta = 1, \varepsilon = 0$) with $Wi = 0.2$

In Figure (1.6), we show contours for $\eta_{el,p}$. The results for the Newtonian case are presented in Figure (1.6a), and those for a UCM fluid with $Wi = 0.2$ in Figure (1.6b). The fore-and-aft and up-and-down symmetries are seen in both cases; this is a consequence of the appearance only of even cosine Fourier modes in the solution (i.e. $\cos(2k\theta)$ where k goes up to 6 for the $O(Wi^4)$ term). Note that the $\cos(4\theta)$ term in the zero-order solution for $\eta_{el,p}$already generates complex structures close to the surface of the cylinder, as one can see in Figure (1.6a). For the viscoelastic case, this situation is intensified not only because of the appearance of high Fourier modes in the high-order terms ($\cos(12\theta)$in the $O(Wi^4)$term) but also because of their combination with terms like $[\ln(r)]^m/r^k$which become maximum (for $m \neq 0$) at a very short distance from the surface of the cylinder. It is more than questionable if such structures can be captured accurately with numerical methods. Indeed, it has often been reported in the literature that very fine meshes are required close to the cylinder for the calculation of the solution with acceptable accuracy, the same holds for the case of a spherical particle too. It is

also worth mentioning that, for both fluids, regions with $\eta_{el,p} < 4$ are observed. These regions shrink in the viscoelastic case and they are located closer to the cylinder compared to the Newtonian fluid. They disappear when the Weissenberg number is increased. We also mention that at fixed Weissenberg number, the exp-PTT model produces smaller values for $\eta_{el,p}$ compared to the UCM/Oldroyd-B models.

Finally, we mention that the rheological parameter ε of the exp-PTT model, appear for the first time in the solution at $O(Wi^2)$. As it is already known, the rheological parameter controls the extensional thickening and shear thinning behavior of the polymeric fluids. These models are also able to predict reasonably well the viscoelastic response of the polymeric fluids even for $Wi > 1/2$ (recall that at $Wi > 1/2$ the UCM/Oldroyd-B models diverge to infinity). Because the effects of the rheological parameters are major only for strongly viscoelastic fluids (i.e. for relatively high values of Wi for which however the perturbation solution is not very accurate), the analytical solutions for these models are valid only for small departures from the UCM/Oldroyd-B models.

In conclusion, whilst the analytical results reported here are lengthy, they are simple and provide a guide for the effects of the viscoelastic properties of the matrix fluid on the flow past a long cylindrical particle. The analytical results, with emphasis on the solution up to 2nd-order in Wi, can be also used as a reference to the accuracy of possible numerical simulations, as well as for the development of new computational methods for viscoelastic flows.

2. STEADY SPHERE TRANSLATION IN A VISCOELASTIC FLUID WITH SLIP ON THE SURFACE OF THE SPHERE

2.1 INTRODUCTION

The steady translation or sedimentation of a spherical particle in a continuous medium is a classical and fundamental fluid mechanics problem important for theoretical, computational, and modelling purposes, as well as for the study of many physical, industrial and real-world applications. The first study of this problem, known as the "falling-ball problem", was presented by Stokes in 1850 [14] under creeping and isothermal flow conditions for a Newtonian fluid. Stokes derived the analytical solution for the pressure and velocity fields around the spherical particle and then by applying a simple force balance on the particle calculated its terminal velocity.

When the surrounding fluid has viscoelastic properties and even in the absence of inertia, the situation is much more complex because the relevant governing equations, i.e. the mass and momentum balances and the constitutive model which describes the mechanical response of the matrix fluid under flow deformation, are strongly non-linear [11]. As such, they cannot be solved analytically unless approximately through a perturbation approach [15] [16] [17], or numerically [6]. In the case of a spherical rigid particle translating with a uniform velocity in a tube there are available in the literature many numerical solutions---see, for example, [7] (Section 9.2) and references therein. This problem has been considered for long time as a benchmark for the evaluation of new numerical methods [7].

However, the usual no slip condition, i.e. the assumption that no slippage arises, at a solid-fluid interface, which is that used in the above works to represent the flow boundary conditions on the solid particle surface, is not always valid. Indeed, the most general condition at a solid-fluid interface should allow for slip, i.e. the possibility

that the adjacent fluid can slip frictionally over a solid surface. Slip is known to occur in several cases, such as the low-density gas flow surrounding an aerosol particle [18], the aqueous liquid flow near a hydrophobic surface [19], and especially the flow of polymer solutions over non-absorbing surfaces [20] [21] [22], polymer melts in tubes and channels [23] [24] [25], and many others, as they have been experimentally confirmed; see the review by Hatzikiriakos [24] and by Malkin and Patlazhan [25] and references therein. The first model of the slipping of a fluid was presented by Navier [26] who assumed that the slip velocity is proportional to the velocity gradient next to the solid surface (known as "Navier law"). The constant of proportionality between the slip velocity and the wall shear stress is called the "slip coefficient." For dilute polymer solutions there are theoretical expressions that provide the slip coefficient as a function of the polymer concentration and polymer properties [21].

The goal of the present work is to investigate how viscoelasticity affects the flow around a spherical particle with slip at the surface of the particle. The flow is assumed creeping, steady, and isothermal. Far from the particle, a uniform velocity stream is applied. No external forces (except from gravity which can be incorporated to the pressure) and torques are applied on the particle, which in conjunction with the symmetries of the flow field implies that the particle does not rotate. Although for a Newtonian fluid the effect of slip has been evaluated in an exact solution that first became available by Basset in 1888 [27], for a viscoelastic fluid this problem has not been studied before in the literature. Note that even for the classical no-slip case, an exact analytical solution of the non-linear governing equations resulting from viscoelasticity is not available. We use here asymptotic methods in order to solve the relevant equations, and in particular we follow the methodology described previously by Housiadas & Tanner [17] adopting a regular perturbation scheme valid for small values of the dimensionless Weissenberg number, Wi (see below for its definition). Thus, we are limited to small departures, up to $O(1)$ in Wi, from the Newtonian response; nonetheless, we expect that the results will also serve as a guide for further numerical exploration of the problem. We solve the resulting sequence of equations analytically up to fourth order in Wi and find the first five terms in the perturbation expansions. Moreover, techniques which accelerate the convergence of series have been utilized in order to increase the range of validity of the asymptotic solutions.

The rest of this chapter is organized as follows. In Section 2.2, we present in dimensionless form the governing equations and the accompanying boundary conditions. In Section 2.3, we present briefly the solution methodology, and the analytical solution for all the dependent primary flow variables up to second order in the Weissenberg number. In Section 2.3, we present the main features of the solution, we comment on the accuracy and validity of the solution, and we discuss the most interesting results. Finally, in Section 2.4 we state the conclusions.

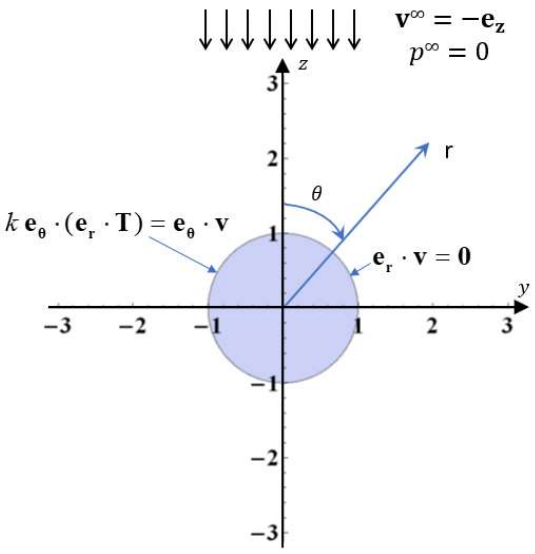

Figure (2.1): Geometry, coordinate systems and dimensionless boundary conditions. Cartesian: xyz with the x axis being normal to the yz plane. Spherical: r, θ, φ where θ is the polar angle $0 \leq \theta \leq \pi$

2.2 GOVERNING EQUATIONS

We consider the translation with a constant speed U of a spherical particle with radius R in an infinite incompressible fluid, with constant mass density ρ. The ambient fluid's rheological behavior is viscoelastic, represented here as the linear combination of a pure Newtonian viscous solvent contribution and that of a polymer solute with zero shear-rate viscosities η_s and η_p, respectively. A single relaxation time is considered for the polymer denoted by λ.

To describe the flow we use spherical coordinates, $r\varphi\theta$, and Cartesian coordinates, xyz; the origin for both coordinate systems is located at the center of the spherical particle as shown in Figure (2.1). The unit vectors of the spherical coordinate system are $\{\boldsymbol{e}_r, \boldsymbol{e}_\theta, \boldsymbol{e}_\phi\}$ and those for the Cartesian system are $\{\boldsymbol{e}_x, \boldsymbol{e}_y, \boldsymbol{e}_z\}$; r is the distance from the center of the sphere, θ is the polar angle ($0 \leq \theta \leq \pi$) and ϕ is the azimuthal angle ($0 \leq \phi < 2\pi$). The velocity vector and the total pressure are denoted by $\mathbf{v}$, p, respectively, and the viscoelastic extra-stress tensor by $\boldsymbol{\tau}$. Far from the spherical body a constant and uniform stream is applied, $v_z^\infty = U$, $v_x^\infty = v_y^\infty = 0$, where throughout the paper the superscript ∞ denotes the far flow-field. The flow is along the z-axis, i.e. the axis of translation of the particle is aligned with the direction of the constant far flow field. The pressure is also constant and taken to be zero, $p^\infty = 0$. We use R for non-dimensionalizing all lengths, U for the velocity, $\mathbf{v}$, components, $(\eta_s + \eta_p)\, U/R$ for the pressure, p, and $\eta_p \;\; U/R$ for the viscoelastic extra-stress, $\boldsymbol{\tau}$, components.

In a Eulerian frame of reference, at steady state, in the absence of external forces and torques, and neglecting inertia, the dimensionless governing equations are:

$$\nabla \cdot \mathbf{v} = 0 \tag{2.1}$$

$$-\nabla p + (1-\eta)\nabla^2 \mathbf{v} + \eta\, \nabla \cdot \boldsymbol{\tau} = \mathbf{0} \tag{2.2}$$

where η is the dimensionless polymer viscosity ratio $\eta \equiv \eta_p/(\eta_s + \eta_p)$. The extra-stress tensor $\boldsymbol{\tau}$ due to viscoelasticity is determined utilizing the exponential Phan-Thien & Tanner (exp-PTT) [28] model:

$$\exp\big(\varepsilon\, Wi\, \mathrm{tr}(\boldsymbol{\tau})\big) + Wi\frac{\delta \boldsymbol{\tau}}{\delta t} = \dot{\boldsymbol{\gamma}} \tag{2.3}$$

where $Wi \equiv U\lambda/R$ is the Weissenberg number, $\dot{\boldsymbol{\gamma}} = \nabla \mathbf{v} + (\nabla \mathbf{v})^T$ is the rate-of-strain tensor, the superscript T denotes the transpose, $\mathrm{tr}(\bullet)$ denotes the trace operator, and $\delta\boldsymbol{\tau}/\delta t$ represents the upper convected derivative of $\boldsymbol{\tau}$ which at steady state is defined as:

$$\frac{\delta \boldsymbol{\tau}}{\delta t} := (\mathbf{v}\cdot\nabla)\boldsymbol{\tau} - \boldsymbol{\tau}\cdot\nabla\mathbf{v} - (\nabla\mathbf{v})^T\cdot\boldsymbol{\tau} \tag{2.4}$$

In Eq.(2.3) ε is additional rheological parameter. For $\varepsilon = 0$ the constitutive model reduce to the Upper Convected Maxwell (UCM) model for $\eta = 1$, to the Newtonian model for $\eta = 0$, and to the Oldroyd-B model for $0 < \eta < 1$; see [11] [22] for more details on the models.

We emphasize here that even for simple flow geometries the UCM and Oldroyd-B models can become singular at a finite Weissenberg number [11]. For instance, for steady uniaxial elongational flow a finite solution exits up to $Wi = 1/2$. This behavior can be easily rectified with the use of more realistic constitutive equations, such as the ePPT model. The disadvantage of these models is that they are more non-linear than the UCM and Olrdoyd-B models (see the exponential term in Eq.(2.3) and it contains more parameters that need to be determined from experimental data. We also mention that the effect of the rheological parameters becomes more apparent for high values of the Weissenberg number, i.e. for strongly viscoelastic fluids.

As we have done before, instead of $\boldsymbol{\tau}$ we work with another second order and symmetric tensor $\boldsymbol{\sigma}$ which is expressed with the aid of $\boldsymbol{\tau}$ and $\dot{\boldsymbol{\gamma}}$:

$$\boldsymbol{\tau} = \dot{\boldsymbol{\gamma}} - Wi\,\boldsymbol{\sigma} \tag{2.5}$$

Of course, the introduction of $\boldsymbol{\sigma}$ does not alter the results. Substituting $\boldsymbol{\tau}$ in Eqs.(2.2)-(2.3), we get, respectively:

$$-\nabla p + \nabla^2\mathbf{v} - \eta\, Wi\ \nabla\cdot\boldsymbol{\sigma} = \mathbf{0} \tag{2.6}$$

$$f\boldsymbol{\sigma} + Wi\frac{\delta\boldsymbol{\sigma}}{\delta t} = \frac{\delta\dot{\boldsymbol{\gamma}}}{\delta t} + \frac{f-1}{Wi}\dot{\boldsymbol{\gamma}}, \quad f = \exp\big(-\varepsilon\, Wi^2\,\mathrm{tr}(\boldsymbol{\sigma})\big) \tag{2.7}$$

The above equations are accompanied with the no-penetration condition on the surface of the rigid particle, and the uniform and constant far flow-field. In the spherical coordinate system these conditions are expressed as follows:

$$v_r(r=1,\theta) = p(r\to\infty,\theta) = 0,$$
$$v_r(r\to\infty,\theta) = -\cos(\theta)\,,\ v_\theta(r\to\infty,\theta) = \sin(\theta) \tag{2.8}$$

As far as the tangential velocity component is concerned, this is imposed implicitly through a Navier-type linear slip condition which in dimensionless form and in terms of the auxiliary stress tensor $\boldsymbol{\sigma}$ is given as:

$$k(\dot{\gamma}_{r\theta} - \eta\, Wi\, \sigma_{r\theta}) = v_\theta \ \text{ at } \ r = 1 \tag{2.9}$$

In the above equation $k \equiv (\eta_s + \eta_p)K/R$ is the dimensionless slip coefficient with K the dimensional slip coefficient with dimensions of length^2 x time / mass and SI units $\mathrm{m}/(\mathrm{Pa\ s})$. For $k = 0$ the usual no-slip condition is recovered while for $k \to \infty$ perfect slip is enforced; the latter implies zero shear forces on the particle. Typical values for the dimensional slip coefficient K are reported by Hatzikiriakos [23], Denn [29], Panaseti [30], and others, in the range $K = 10^{-5} - 10^{-3}\ \mathrm{m}/(\mathrm{Pa\ s})$. Considering a typical viscoelastic polymer solution (whose total viscosity is usually larger than 1 Pa s) and spherical particles with a few millimeters diameter, the dimensionless slip coefficient varies in the range $0.001 < k < 1$. Here, we conduct a parametric investigation of the effect of k on the flow field and the drag force on the particle.

The domain of definition of the governing equations is $1 < r < \infty,\ 0 < \theta < \pi,\ 0 \le \phi < 2\pi$; however as the flow is axisymmetric there is no-dependence of the primary flow variables p, $\mathbf{v}$ and $\boldsymbol{\tau}$ (or $\boldsymbol{\sigma}$) on the azimuthal angle ϕ. Thus, the final equations are seven scalar partial differential equations in two spatial dimensions (r and θ). Finally, we mention that the constant far flow-field leads to zero rate-of-strain tensor $\dot{\boldsymbol{\gamma}}^{\infty} = \mathbf{0}$ and zero constant extra-stress tensor $\boldsymbol{\sigma}^{\infty} = \mathbf{0}$. Note that with the method of solution used here boundary conditions for $\boldsymbol{\sigma}$ are not required (and cannot be imposed). They are only used a-posteriori, after the analytical solution has been calculated, as an independent check of the correctness of the solution.

2.3 SOLUTION METHODOLOGY

The method of solution, and the solution procedure, has been described in [17]. For completeness, we briefly mention here the main features. We use a regular perturbation scheme in terms of the Weissenberg number, i.e. the solution for all the dependent variables is given as a power series expansion in terms of Wi:

$$X \approx X_0 + Wi\, X_1 + Wi^2\, X_2 + \ldots, \quad X = \mathbf{v}, p, \boldsymbol{\sigma} \tag{2.10}$$

where the zero-order term, X_0, corresponds to the solution for the simple Newtonian fluid. Note that for weakly viscoelastic fluids, only regular perturbation schemes should be employed, as it has explained and discussed in detail by Brid et al. [11] and Hassager et al. [15]. The upper convected derivative depends linearly on $\mathbf{v}$ and $\nabla\mathbf{v}$, and it is expanded as follows:

$$\frac{\delta(\bullet)}{\delta t} = \sum_{j=0} Wi^j \frac{\delta_j(\bullet)}{\delta t},$$
$$\frac{\delta_j(\bullet)}{\delta t} := \mathbf{v}_j \cdot \nabla(\bullet) - (\bullet)\cdot\nabla\mathbf{v}_j - \left(\nabla\mathbf{v}_j\right)^T \cdot (\bullet) \tag{2.11}$$

Expressions (2.10)-(2.11) are substituted in the governing equations and a sequence of equations at $O(Wi^j)$, $j = 0,1,2,\ldots$ results. Introducing $\boldsymbol{\sigma}_{-1} = \mathbf{0}$ for completeness, the mass balance, momentum balance and the Poission-type equation for the pressure are:

$$\begin{aligned} \nabla \cdot \mathbf{v}_j &= 0, \\ -\nabla p_j + \nabla^2 \mathbf{v}_j &= \eta\, \nabla \cdot \boldsymbol{\sigma}_{j-1}, \\ \nabla^2 p_j + \eta\, \nabla \cdot \left(\nabla \cdot \boldsymbol{\sigma}_{j-1}\right) &= 0 \end{aligned} \tag{2.12}$$

Eq. (2.12c) is derived by taking the divergence of Eq. (2.12b) in conjunction with the continuity equation Eq. (2.12a). It is not an independent equation but is used only because it facilitates the solution procedure. Notice that Eqs. (2.12) contain only two unknowns, $\mathbf{v}_j$ and p_j, since the auxiliary extra-stress tensor $\boldsymbol{\sigma}_{j-1}$ is found from the constitutive models, Eq.(2.7), in terms of the solution at the previous orders in Wi. For $j = 0$ Eqs. (2.12) reflect the equations for a simple Newtonian fluid and can be easily solved analytically recovering the Basset solution [27]. In spherical coordinates and components, the solution is:

$$\begin{aligned} v_{r,0} &= \left(-1 + \frac{c_0}{r} + \frac{1-c_0}{r^3}\right)\cos(\theta), \\ v_{\theta,0} &= \left(1 - \frac{c_0}{2r} + \frac{1-c_0}{2r^3}\right)\sin(\theta), \\ p_0 &= \frac{c_0}{r^2}\cos(\theta) \end{aligned} \tag{2.13}$$

Where

$$c_0 = \frac{3(1+2k)}{2(1+2k)} \tag{2.14}$$

For $k \to 0$, $c_0 \to 3/2$ and Eqs.(2.13) reduces to the well-known Stokes solution [14]. It can be trivially confirmed that Eq.(2.13) satisfies the far flow-field conditions and the zero radial velocity component on the surface of the particle $\left(v_{r,0}(r=1,\theta)=0\right)$. Note that $\partial v_{r,0}/\partial r\big|_{r=1} = (2c_0 - 3)\cos(\theta) \neq 0$ unless when $k \to 0$.

When the zero-order term is in the form shown by Eq. (2.13) , the higher-order in Wi sequence of equations reduces to a set of ordinary differential equations that can be solved analytically using standard methods. We also mention here that the solution procedure is equivalent to the method of separation of variables. Eqs (2.12) are solved sequentially for $j = 1, 2, 3$ and 4 namely the solution is derived analytically for all the field variables up to $O(Wi^4)$. At orders higher than one, this task is achieved by developing a symbolic code with the "Mathematica" software [12] with the aid of which the solution is also checked for its correctness. The 1st order solution for the UCM ($\eta = 1$) and Oldroyd-B ($0 < \eta < 1$) models is given as:

$$p_1 = \eta \left\{ \begin{array}{c} \left(\frac{9(1-c_0)^2}{r^8} + \frac{23(1-c_0)c_0}{4r^6} + \frac{3c_0^2}{2r^4} + \frac{c_1}{6r^3} \right) \\ + \left(\frac{9(1-c_0)^2}{2r^8} + \frac{21(1-c_0)c_0}{4r^6} + \frac{5c_0^2}{2r^4} + \frac{c_1}{2r^3} \right) \cos(2\theta) \end{array} \right\},$$

$$v_{r,1} = \eta \left\{ \begin{array}{c} \frac{(1-c_0)c_0}{4r^5} + \frac{c_0^2}{4r^3} - \frac{6c_0^2 + c_1}{12r^4} + \frac{3c_0 + c_1}{12r^2} \\ + \left(\frac{3(1-c_0)c_0}{4r^5} + \frac{3c_0^2}{4r^3} - \frac{6c_0^2 + c_1}{4r^4} + \frac{3c_0 + c_1}{4r^2} \right) \cos(2\theta) \end{array} \right\}, \tag{2.15}$$

$$v_{\theta,1} = \eta \left(\frac{3(1-c_0)c_0}{4r^5} + \frac{c_0^2}{4r^3} - \frac{c_0^2 + c_1/6}{r^4} \right) \sin(2\theta),$$

where

$$c_1 = -\frac{27(1 + 10k + 26k^2 + 32k^3)}{4(1+3k)^2(1+5k)} \tag{2.16}$$

Regarding the exp-PTT model, we mention that a nonzero value for the rheological parameter ε does not modify the solution Eqs.(2.15)-(2.16).

At second order in Wi, the solution for the UCM and Oldroyd-B models can be compactly expressed as:

$$p_2 = \eta \left(G_1 \cos(\theta) + G_3 \cos(3\theta) \right)$$

$$v_{r,2} = \eta \left(F_1 \cos(\theta) + F_3 \cos(3\theta) \right)$$

$$v_{\theta,2} = \eta \left\{ \begin{array}{c} \left(\frac{F_3}{2} - F_1 + \frac{r}{2} \left(\frac{F_3'}{2} - F_1' \right) \right) \sin(\theta) \\ -\frac{1}{2} \left(F_3 + r \frac{F_3'}{2} \right) \sin(3\theta) \end{array} \right\}. \tag{2.17}$$

The G_1, G_3, F_1, F_3 are functions of the radial distance r, given as follows:

$$F_1(r) = \frac{9\,(1+\eta)\,c_0^3}{35} \frac{\ln(r)}{r^5} + \frac{c_2}{r} + \sum_{k=3}^{9} \frac{f_{1,k}}{r^k} + \frac{81\,(c_0-1)^3}{572\,r^{11}},$$

$$F_3(r) = \frac{3\,(1+\eta)\,c_0^3}{7} \frac{\ln(r)}{r^5} + \sum_{k=3}^{9} \frac{f_{3,k}}{r^k} + \frac{3\,(c_0-1)^3}{52\,r^{11}}, \tag{2.18}$$

$$G_1(r) = \frac{c_2}{r^2} + \frac{3c_3}{20\,r^4} + \sum_{k=5}^{10} \frac{g_{1,k}}{r^k} + \frac{5643\,(c_0-1)^3}{104\,r^{12}},$$

$$G_3(r) = \frac{c_3}{4\,r^4} + \sum_{k=5}^{10} \frac{g_{3,k}}{r^k} + \frac{81\,(c_0-1)^3}{8\,r^{12}}$$

and $f_{1,k}, f_{3,k}, g_{1,k}, g_{3,k}$, $k = 3,4,\ldots,10$ are constants which are provided in the Appendix B. Worth mentioning is the appearance in Eqs.(2.17)-(2.18) of the term $\ln(r)/r^5$ in the velocity profile. The solution becomes even more complicated at higher orders in Wi .

SECONDARY FLOW VARIABLES

Based on the perturbation scheme, and at any order $j = 0,1,2,3$, in the Weissenberg number, the rate-of-strain tensor is given simply by $\dot{\boldsymbol{\gamma}}_j = \nabla\mathbf{v}_j + \left(\nabla\mathbf{v}_j\right)^T$, while the extra-stress tensor due to the viscoelasticity of the fluid becomes $\boldsymbol{\tau}_j = \dot{\boldsymbol{\gamma}}_j - \boldsymbol{\sigma}_{j-1}$ where $\boldsymbol{\sigma}_{j-1}$ is found using any of the constitutive models; recall that $\boldsymbol{\sigma}_{-1} = \mathbf{0}$. Also, a stream function $\Psi = \Psi(r,\theta)$ can be defined as follows:

$$v_r = -\frac{1}{r^2\,\sin(\theta)}\frac{\partial\Psi}{\partial\theta}, \quad v_\theta = \frac{1}{r\,\sin(\theta)}\frac{\partial\Psi}{\partial r} \tag{2.19}$$

Integrating Eq.(2.19b) gives $\Psi(r,\theta) - \Psi(1,\theta) = \sin(\theta)\int_1^r \tilde{r}\; v_\theta(\tilde{r},\theta)\,d\tilde{r}$. From Eq.(17a) and the boundary condition, Eq.(2.8), we conclude that $\Psi(1,\theta)$ is a constant, i.e. there is no dependence on θ. Since only the stream function differences are of interest, we arbitrarily set $\Psi(1,\theta) = 0$. Using the analytical solution for $v_{\theta,j}$, we can find Ψ_j, $j = 0,1,2,3,4$, but since the higher order expressions are lengthy, we report only the zero- and first-order terms:

$$\begin{aligned}
\Psi_0 &= \frac{\sin^2(\theta)}{2}\left(r^2 - c_0 r + \frac{c_0-1}{r}\right) \\
\Psi_1 &= \eta\,\frac{\cos(\theta)\sin^2(\theta)}{8}\left(\frac{(1-c_0)\,c_0}{r^3} - \frac{c_0^2}{r} + \frac{6\,c_0^2 + c_1}{3r^2} - c_0 - \frac{c_1}{3}\right)
\end{aligned} \tag{2.20}$$

As far as the vorticity vector $\boldsymbol{\omega} \equiv \nabla\times\mathbf{v}$ is concerned, one finds $\boldsymbol{\omega} = \omega_\phi\mathbf{e}_\phi$. The zero- and first-order terms are:

$$\begin{aligned}
\omega_{\phi,0} &= \frac{c_0\,\sin(\theta)}{r^2} \\
\omega_{\phi,1} &= \frac{3\eta}{2r^3}\left(\left(\frac{1}{r^3}+1\right)c_0 + \left(\frac{1}{3}-\frac{1}{r^2}\right)\frac{c_0^2}{r} + \frac{c_1}{3}\right)\sin(2\theta)
\end{aligned} \tag{2.21}$$

Lastly, we report the conformation tensor $\mathbf{c}$, which represents the second moment of the end-to-end position vector of all possible internal configurations that the polymer molecules can take due to the flow deformation

[22]. For the constitutive models used here $\mathbf{c}$ and $\boldsymbol{\tau}$ are connected as $\boldsymbol{\tau} = (\mathbf{c} - \mathbf{I})/Wi$. The latter combined with $\boldsymbol{\tau} = \dot{\boldsymbol{\gamma}} - Wi\,\boldsymbol{\sigma}$, $\mathrm{tr}(\dot{\boldsymbol{\gamma}}) = 0$ and $\mathrm{tr}(\mathbf{I}) = 3$ gives:

$$\mathbf{c} = \mathbf{I} + Wi\,\dot{\boldsymbol{\gamma}} - Wi^2\boldsymbol{\sigma}, \quad \mathrm{tr}(\mathbf{c}) = 3 - Wi^2 \tag{2.22}$$

Using the perturbation scheme, Eq.(2.22b) gives $\mathrm{tr}(\mathbf{c}) \approx 3 - Wi^2\ \mathrm{tr}(\boldsymbol{\sigma}_0)$ where $\boldsymbol{\sigma}_0 = \boldsymbol{\sigma}_0(\mathbf{v}_0)$. It is worth mentioning that at any order in the Weissenberg number, the conformation tensor and its trace can be calculated up to two orders in the Weissenberg higher than the velocity and pressure fields; see also [17]. For $\mathrm{tr}(\boldsymbol{\sigma}_0)$, the solution for the UCM and Oldroyd-B models is:

$$\mathrm{tr}(\boldsymbol{\sigma}_0) = -18\left\{\begin{array}{c}\left(\dfrac{2\,(c_0-1)^2}{r^8} - \dfrac{(c_0-1)\,c_0}{r^6} + \dfrac{c_0^2}{6r^4}\right) \\ +\left(\dfrac{(c_0-1)^2}{r^8} - \dfrac{(c_0-1)\,c_0}{r^6} + \dfrac{c_0^2}{6r^4}\right)\cos(2\theta)\end{array}\right\} \tag{2.23}$$

Regarding the exp-PTT model, ε does not affect the solution at first order.

DRAG ON THE SPHERE

A major quantity of interest for this type of flow is the total force $\mathbf{D}$ that the fluid exerts on the particle. It can be found by integrating the traction vector $\mathbf{T} \cdot \mathbf{e_r}$ on the surface of the particle. Due to the uniform far-flow field and the symmetries of the spherical particle, one can easily show that $\mathbf{D} = -D\mathbf{e_z}$ with

$$D \equiv \frac{\widetilde{D}}{6\pi\,(\eta_s + \eta_p)R\,U} > 0 \tag{2.24}$$

where $\widetilde{D}$ is the total dimensional drag force, i.e. there is only a non-zero component of the force acting on the particle which is along the z-axis. The final formula is:

$$D = D_P + D_V + D_E \tag{2.25}$$

where

$$D_P = \frac{1}{6}\int_0^{\pi} p\,\sin(2\theta)\,d\theta$$

$$D_V = \frac{1}{3}\int_0^{\pi}\left(\left(\frac{\partial v_\theta}{\partial r} - v_\theta\right)\sin(\theta) - 2\frac{\partial v_r}{\partial r}\cos(\theta)\right)\sin(\theta)\,d\theta \tag{2.26}$$

$$D_E = \frac{\eta\,Wi}{3}\int_0^{\pi}(\sigma_{rr}\cos(\theta) - \sigma_{r\theta}\sin(\theta))\sin(\theta)\,d\theta$$

All quantities in Eqs.(2.20) are evaluated at $r = 1$. Notice the three distinct contributions, namely the form drag, D_P, due to the isotropic pressure, the friction drag, D_V, due to the viscous stresses, and the elastic drag, D_E, due to the viscoelasticity of the polymer. Note that the elastic drag contribution D_E is an $O(Wi)$ quantity. Substituting $\mathbf{v}_0$ (see Eq.(2.13)) and $\boldsymbol{\sigma}_0 = \boldsymbol{\sigma}_0(\mathbf{v}_0)$ in Eqs.(2.20) gives the lowest-order terms for D_P, D_V and D_E, respectively:

$$D_0 = \frac{1+2k}{1+3k}, \quad D_{P,0} = \frac{1+2k}{3(1+3k)}, \quad D_{V,0} = \frac{2(1+2k)}{3(1+3k)}, \quad D_{E,0} = 0 \tag{2.27}$$

These correspond to the Newtonian fluid Basset solution [27]. Note that, as commented by Premlata & Wei [31], the Basset solution is identical to the Hadamard [32] and Rybczynski [33] formula for the steady drag on a spherical drop when the dimensionless slip coefficient k is taken as the one third of the viscosity ratio of the bulk fluid to the drop [Crowe & Michaelides, [34]]. This correspondence between the slip coefficient k and the effective viscosity ratio, of the bulk fluid to the drop, also holds when the effective viscosity of a dilute suspension is considered. However, there the proportionality constant turns out to be different, one fifth [35].

For $k \to 0$ the Stokes results, i.e. $D_0 = 1$, $D_{P,0} = 1/3$ and $D_{V,0} = 2/3$, are recovered. Eq.(2.27) shows that as the dimensionless drag coefficient k increases the total drag, and its individual contributions, drop monotonically. Since $k \geq 0$, the dimensionless drag force varies in the window $2/3 \leq D \leq 1$, namely the slippage of the fluid on the surface of the particle reduces the applied force on the particle. It is also interesting the fact that the $O(Wi)$ term of the elastic drag is zero, i.e. the integral of D_E in Eq.(2.26) based on $\sigma_{rr,0}(r = 1, \theta)$ and $\sigma_{r\theta,0}(r = 1, \theta)$ is zero.

The first correction to the Newtonian solution is of second-order in Wi, i.e. $D_2 = D_{P,2} + D_{V,2} + D_{E,2}$, and is given for the UCM and Oldroyd-B fluids as:

$$D_2 = \frac{\eta\left(d_{2,1} + d_{2,2}\eta\right)}{(1+3k)^4(1+5k)},$$
$$d_{2,1} = \begin{Bmatrix} -0.0103 - 0.1855k - 1.4072k^2 \\ -0.4971k^3 + 22.4228k^4 + 32.4k^5 \end{Bmatrix}, d_{2,2} = \begin{Bmatrix} -0.0057 - 0.1028k - 0.78k^2 \\ +1.5314k^3 + 1.8514k^4 - 7.2k^5 \end{Bmatrix} \tag{2.28}$$

The corresponding formulae for the full exp-PTT model are provided in the Appendix B. The next term is of fourth order, $D_4 = D_{P,4} + D_{V,4} + D_{E,4}$, and can be written as:

$$D_4 = \left\{ \begin{array}{c} \dfrac{\eta\, d_{4,1}}{(1+3k)^6} + \dfrac{\eta^2 d_{4,2}}{(1+3k)^7(1+5k)(1+7k)} \\ + \dfrac{\eta^3 d_{4,3}}{(1+3k)^7(1+5k)^2(1+7k)} \\ + \dfrac{\eta^4 d_{4,4}}{(1+3k)^7(1+5k)^3(1+7k)} \end{array} \right\} \tag{2.29}$$

where the constants $d_{4,1}, d_{4,2}, d_{4,3}$ and $d_{4,4}$ are provided in the Appendix B. Thus, the total drag force on the particle based on the perturbation scheme is:

$$D \approx D_0 + D_2 Wi^2 + D_4 Wi^4 \tag{2.30}$$

As expected, and previously found for other flow problems past spheres [17], only the even orders in Wi contribute. Furthermore, and provided that $|D_2|$ is not much smaller than $|D_4|$, an expression with increased accuracy can be found by applying Shanks non-linear transformation [36] [10] [37] which yields:

$$D_{S,4} \approx D_0 + \frac{Wi^2 D_2^2}{D_2 - Wi^2 D_4} \tag{2.31}$$

where the subscript S denotes the Shanks transformation, and the numerical index, 4, denotes that the solution up to $O(Wi^4)$ has been taken into account to construct the transformation. Hereafter, we will refer to Shanks transformation as the "convergence acceleration technique" used in order to increase the accuracy and extend the domain of convergence of the original perturbation results. Eq.(2.31) shows that when both D_2 and D_4 have the same sign, Shanks transformation is valid up to $Wi_c = \sqrt{D_2/D_4}$. One cannot easily determine whether Wi_c is a spurious pole of the solution, a real singular point, or an approximation of a real singular point. The improved accuracy and efficiency of Shanks transformation for viscoelastic flow problems past spheres and cylinders, especially when only the first three terms are used, as in Eq.(2.31), has been confirmed in Refs [37] [8] [38] by comparing the accelerated asymptotic results with the corresponding analytical solutions [37] or with the numerical results from the literature [8] [38]. We also mention here that the minimum number of terms needed in order to implement an acceleration technique on a series is there. When more terms in the original series solution are available other transformation methods can be also applied such as Euler transformation (see also below in subsection Accuracy of the solution), or the multiple-level Shanks transform and the Padé-type approximants as it has been extensively studied in Ref. [37].

2.4 CORRECTNESS, VALIDITY AND ACCURACY OF THE SOLUTION

CONSISTENCY CHECKS

The correctness of our analytical perturbation solution is checked with the aid of the "Mathematica" software [12] by performing the following consistency tests, all of which were successfully passed, valid at any order in the Weissenberg number, j:

(a) The first test is based on the continuity equation which can be integrated to give:

$$\int_0^{\pi} v_{r,j}(r,\theta)\sin(\theta)\,d\theta = 0, \quad 1 \le r < \infty \tag{2.32}$$

(b) The second test is based on the momentum balance, Eq.(2.12b), which has two non-trivial components; in the radial and polar angle of the spherical coordinate system (r, θ, respectively). However, the θ-component of the momentum balance is not really used. Indeed, according to the solution procedure, p_j

is determined solving Eq.(2.12c), $v_{\theta,j}$ is found in terms of $v_{r,j}$ solving Eq.(2.12a), and finally $v_{r,j}$ is found solving the radial component of Eq.(2.12b). Thus, substituting the solution for all variables in the θ-component of the momentum balance provides an independent test of its correctness.

(c) The third test is based on the far flow-field viscoelastic extra-stress tensor $\boldsymbol{\sigma}^{\infty}$ which is calculated simply by substituting $\mathbf{v}^{\infty}$ in the constitutive model(s) and solving the resulting equations. Then, $\boldsymbol{\sigma}^{\infty}$ can be expanded and found in series form as $\boldsymbol{\sigma}^{\infty} = \sum_{j=0} \boldsymbol{\sigma}_j^{\infty}\, Wi^j$. However, due to the method of solution used here, $\boldsymbol{\sigma}_j^{\infty}$ cannot be imposed because at any order in Wi $\boldsymbol{\sigma}_j$ is fully determined using all the lower-order solutions (i.e. $\mathbf{v}_0, \mathbf{v}_1, \ldots, \mathbf{v}_{j-1}$) and the constitutive model(s) without the need to solve differential equations (see Ref. [17] for more details). Comparing $\boldsymbol{\sigma}_j(r \to \infty)$ with $\boldsymbol{\sigma}_j^{\infty}$ gives another undeniable test of the correctness of the analytical solution at any order in the Weissenberg number.

(d) The fourth and final test is based again on the momentum balance. Since the dimensionless total stress tensor is given by the expression $\mathbf{T} = -p\mathbf{I} + (1-\eta)\dot{\boldsymbol{\gamma}} + \eta\, \boldsymbol{\tau}$, the introduction of the new tensor $\boldsymbol{\sigma}$ results to $\mathbf{T} = -p\mathbf{I} + \dot{\boldsymbol{\gamma}} - \eta\, Wi\, \boldsymbol{\sigma}$. Thus, at any order in the Weissenberg number, $\mathbf{T}$ is given as $\mathbf{T}_j = -p_j\mathbf{I} + \dot{\boldsymbol{\gamma}}_j - \eta\, \boldsymbol{\sigma}_{j-1}$. Also, the momentum balance, Eq.(2.2), or Eq.(2.6), simply becomes:

$$\nabla \cdot \mathbf{T}_j = \mathbf{0} \tag{2.33}$$

Choosing a fluid volume V which is enclosed between the surface of the sphere and an imaginary sphere with radius $r > 1$, integrating Eq.(2.33) over V, i.e. $\int_V \nabla \cdot \mathbf{T}_j\, dV = \mathbf{0}$, applying the divergence theorem to convert the volume integral to a surface integral, and using spherical coordinates, gives

$$\int_{\theta=0}^{\pi}\int_{\phi=0}^{2\pi} (\mathbf{e_r} \cdot \mathbf{T} s^2 \sin(\theta))_{s=1} d\theta d\phi = \int_{\theta=0}^{\pi}\int_{\phi=0}^{2\pi} (\mathbf{e_r} \cdot \mathbf{T} s^2 \sin(\theta))_{s=r} d\theta d\phi\,, \quad 1 \le r < \infty \tag{2.34}$$

The constant quantity on the left-hand-side of Eq.(2.34) is merely the dimensionless total force $-\mathbf{D}$ that the fluid exerts on the spherical particle. Thus, the right-hand-side of Eq.(2.34) should be independent of the radial distance r. Indeed, this has been confirmed based on the analytical solution up to $O(Wi^4)$.

VALIDITY OF THE SOLUTION

An important feature of the real, symmetric and second-order conformation tensor, $\mathbf{c}$, is its positive definite character [22] [13]. This implies that all its eigenvalues, and consequently its trace which equals the sum of the eigenvalues, are strictly positive, a property which is necessary for the results to have physical meaning. This can be used to check the validity of an approximate solution. This issue has also been discussed extensively for the flow past an infinitely long cylinder by Housiadas & Tanner [8], for simple shear flow. For a two-dimensional and axisymmetric flow field expressed in spherical coordinates we have $c_{\theta\phi} = c_{r\phi} = 0$, $c_{\phi\phi} = 1$, while necessary conditions for positive definiteness are $c_{rr} > 0$, $c_{\theta\theta} > 0$ and $c_{rr}\, c_{\theta\theta} - c_{r\theta}^2 > 0$. We focus however on the trace of the conformation tensor and use it as a guidance of the validity and accuracy of the

velocity/pressure fields. Note that in the following discussion the full available perturbation solution up to $O(Wi^5)$ and $O(Wi^4)$, respectively, are used.

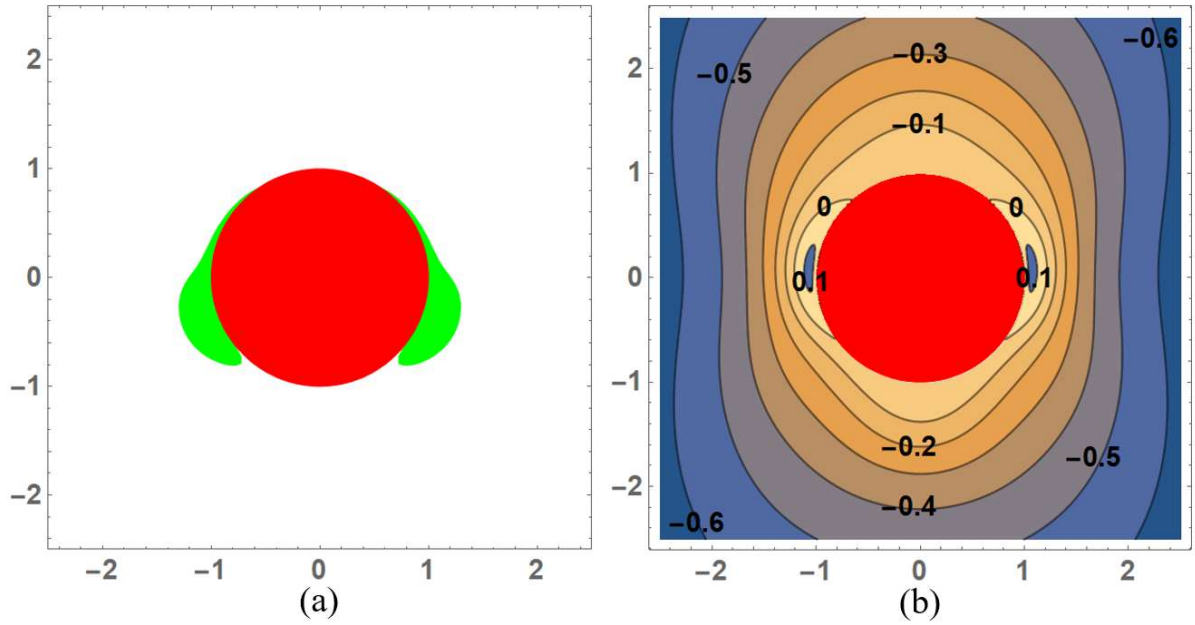

Figure (2.2): exp-PTT model with $Wi = 1.5$, $\eta = 0.4$, $\varepsilon = 0.3$ and no-slip ($k = 0$)

(a) Regions with $\mathrm{tr}(\mathbf{c}) < 0$, (b) Axial velocity

For the limiting case as the slip coefficient k goes to zero, namely for the classic no-slip boundary condition on the particle, Housiadas & Tanner [17] identified that for the exp-PTT and UCM/Oldroyd-B models, a negative trace of the conformation tensor close to the surface of the sphere results in artificial negative wakes, i.e. in flow regions with sign of the axial velocity component which was the opposite than its far-flow field sign. This situation is presented in Figure (2.2) for the exp-PTT model based on results obtained in this work. The Weissenberg number is rather large, $Wi = 1.5$, the polymer viscosity ratio is $\eta = 0.4$, the rheological parameter is $\varepsilon = 0.3$, and the classical no-slip condition is applied ($k = 0$). In Figure (2.2a), the colored (green) region, which is located around the sphere away from the poles ($\theta = 0$ and $\theta = \pi$) and near the equator ($\theta = \pi/2$) indicates a negative trace of the conformation tensor. In this region, approximately, the contours for the axial velocity component $v_z = \mathbf{e_z} \cdot \mathbf{v}$ which are presented in Figure (2.2b) clearly show that $v_z > 0$, i.e. a negative wake is identified. In conjunction with the fact that when $\mathrm{tr}(\mathbf{c}) > 0$ everywhere in the flow, no negative wakes are predicted, we conclude that for creeping flow the negative wake is an artificial result accompanying that of the loss of positive definiteness of the conformation tensor, indicative of a loss of validity for the perturbation approximation at that high value of Wi.

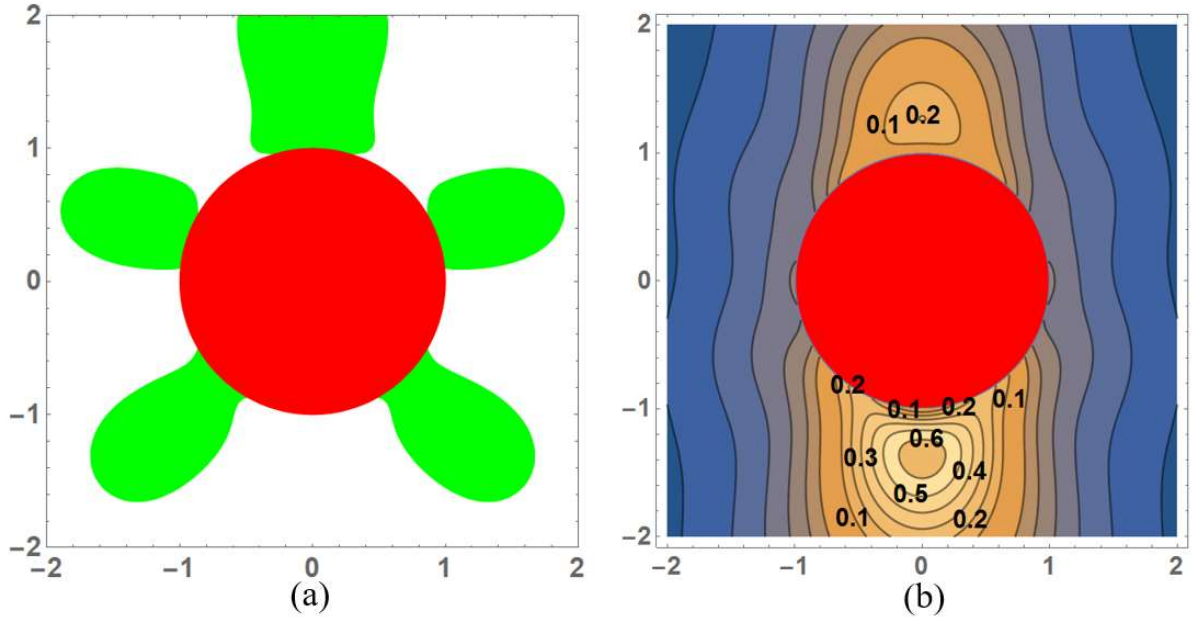

Figure (2.3): Oldroyd-B model with $Wi = 1.5$, $\eta = 0.4$ and perfect slip ($k \to \infty$)

(a) Regions with $\mathrm{tr}(\mathbf{c}) < 0$, (b) Axial velocity

We also investigated the prediction of negative wakes under perfect slip conditions ($k \to \infty$) in Figure (2.3). We have chosen to present there the Oldroyd-B model with $\eta = 0.4$ and $Wi = 1.5$. For this model and for the same parameters, the no-slip case does not reveal neither any flow regions with $\mathrm{tr}(\mathbf{c}) < 0$, nor negative wakes. However, the situation for perfect slip on the sphere is quite different, as Figure (2.3) clearly shows. Indeed, extensive regions with $\mathrm{tr}(\mathbf{c}) < 0$ are predicted around the sphere. Decreasing the Weissenberg number, the regions with negative trace, and those with negative wakes, gradually shrink and for $Wi \approx 0.9$ are eliminated. Obviously, the negative wakes are closely related to the loss of positive definiteness of the conformation tensor.

All these observations are consistent with the fact that as the small parameter of the perturbation scheme increases, the original perturbation solution gradually loses its accuracy and validity. We have not implemented an acceleration convergence scheme in field quantities since no such scheme is available in contrast to integral quantities like the drag force. Note that in the following we present results for Wi number and rheological parameters such that the conformation tensor is everywhere (or almost everywhere) positive definite. In any case, it is important to note that at least for the UCM and Oldroyd-B cases, the steady state solution is not expected to exist for all Wi numbers due to the previously mentioned singularity present in those models. In fact, all numerical methods encounter problems of convergence for high enough Wi numbers; how high someone can go depends on the flow geometry (numerical calculations are typically carried out for a sphere moving within a cylinder) and the viscosity ratio. For example, for UCM fluid and a ratio of sphere/cylinder radius of 0.5 it appears that convergence is lost at some point after $Wi = 1.5$; see Table 9.2 in Ref. [7].

ACCURACY OF THE SOLUTION

We have used the total drag on the particle for the no-slip case ($k = 0$) and the UCM model ($\eta = 1$) which has been found by Housiadas & Tanner [17] up to $O(Wi^8)$ in order to test the accuracy of our fourth order solution. For additional accuracy, we have also calculated the $O(Wi^{10})$ term, a task which pushed the software and the computer to their limits. Truncating the results in 5 significant digits we find:

$$D_{\langle 10\rangle} = 1 + \begin{pmatrix} -1.6024 + 1.2155\ Wi^2 - 0.63995\ Wi^4 \\ +0.47452\ Wi^6 - 0.53612 Wi^8 \end{pmatrix} Wi^2 \times 10^{-2} \tag{2.35}$$

where hereafter the notation $D_{\langle k\rangle} := \sum_{n=0}^{k} D_n Wi^n$ is used. Since the series is alternating, first we use Euler's linear transformation as a method to accelerate its convergence as previously has been implemented successfully for a variety of simple viscoelastic flow problems by Housiadas [37]. Using the 5 and 6 first terms in Eq.(2.35), we find, respectively:

$$D_{E,8} = 1 + (-1.5022 + 0.83563 Wi^2 - 0.19998 Wi^4 + 0.029658 Wi^6) Wi^2 \times 10^{-2} \tag{2.36}$$

$$D_{E,10} = 1 + \begin{pmatrix} -1.5523 + 0.98757\ Wi^2 - 0.31998\ Wi^4 \\ +0.088973\ Wi^6 - 0.016754\ Wi^8 \end{pmatrix} Wi^2 \times 10^{-2} \tag{2.37}$$

where the subscript E denotes Euler's linear transformation and the numerical index the order of the original series used. Note that the magnitude of the coefficients of the transformed series decreases much faster than those of the original series which is an indication for faster convergence too.

Shanks' non-linear transformation, Eq.(2.31), is employed extensively in our work as the method for convergence acceleration given the limited order (4^{th}) of the available perturbation solution. Using only the first 3 terms in Eq.(2.35) gives:

$$D_{S,4} = 1 - \frac{0.0256768\ Wi^2}{1.6024 + 1.21547\ Wi^2} \tag{2.38}$$

The results are shown as a function of the Weissenberg number in Figure (2.4). First, focusing on the original series, Eq.(2.35), one notices that as more terms are included in the series, convergence at a higher Weissenberg number is observed; note however that the convergence is slow. For $D_{\langle 2\rangle}$ convergence has been achieved up to $Wi{\sim}0.3$, for $D_{\langle 4\rangle}$ increases up to $Wi{\sim}0.6$, but one has to go up to $D_{\langle 10\rangle}$ to observe convergence up to $Wi{\sim}0.8$. In contrast, the convergence of the accelerated series, Eq.(2.36) and (2.37), is much faster. For $D_{S,4}$ we get as good results, or even better, than for $D_{\langle 10\rangle}$, whereas for $D_{E,8}$ and $D_{E,10}$ one observes convergence up to $Wi{\sim}1.4$. Comparing $D_{S,4}$ with $D_{E,8}$ and $D_{E,10}$, convergence up to $Wi{\sim}1.0$ can be confirmed; this is substantially higher (almost doubled) than what is observed with the original $D_{\langle 4\rangle}$. This justifies the use of the acceleration method in presenting the predictions for the drag in the "Results and discussion" section.

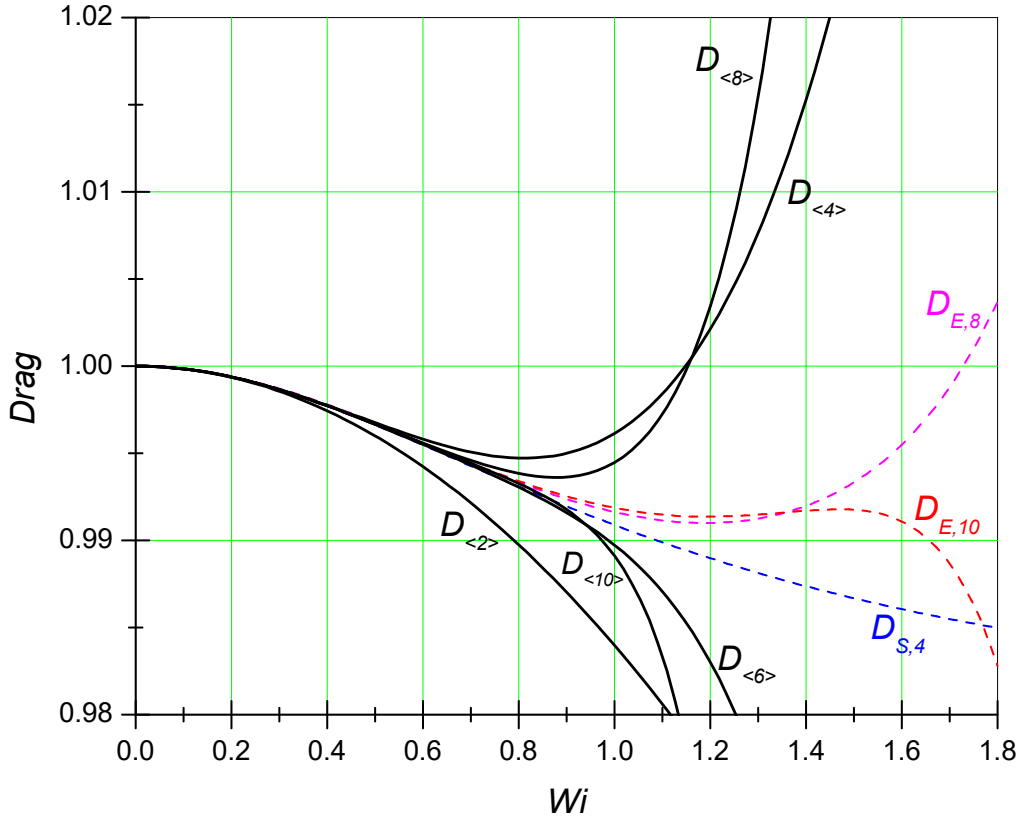

Figure (2.4): Normalized drag force for ***no-slip*** ($k = 0$) for the UCM model ($\eta = 1$).
Black solid lines: perturbation results up 2nd ,4th, 6th, 8th and 10th order in Wi from Eqs.(2.35)-(2.38).
Dashed lines: accelerated results based on Eqs (2.31), (2.36)-(2.37) for $D_{S,4}$, $D_{E,8}$ and $D_{E,10}$, respectively.

We also compare our perturbative analytical results with the available numerical results from the literature. For the models used in the present work and even for the no-slip case, numerical results are only available for the confined sphere problem in a cylinder. As far as we are aware of, for the no-slip case, the best compromise appears to be the finite element calculations for the Oldroyd-B model with $\eta = 8/9$ by Bodart & Crochet [39] who demonstrated numerical convergence with three different mesh sizes up to $Wi = 2$. We use their normalized drag results for the smallest ratio of sphere to cylinder radii (0.02) which appear to have converged as far as the effect of the confinement ratio is concerned. In fact, for that ratio the simulations correspond to an unbounded flow domain. In Figure (2.5), we compare their drag predictions, normalized by the corresponding to the same confinement Newtonian value, against our own results. In particular, we show the original series solution up to fourth order in Wi, i.e. the quantity $D_{\langle 4\rangle}$ (following Eq.(2.39) below), and its transformed expression according to Eq.(2.31), $D_{S,4}$, as well as the Euler transformations $D_{E,8}$ and $D_{E,10}$. It is seen that all transformations are converged up to $Wi{\sim}1.0$ while the original series, $D_{\langle 4\rangle}$, agrees well with the numerical results only up to $Wi{\sim}0.6$. Worth mentioning is that $D_{E,8}$ overlaps with the numerical results up to $Wi{\sim}1.8$.

However, the next approximation $D_{E,10}$ begins to fail at $Wi{\sim}1.4$. These observations fully justify the methods and the order of approximation used as the best compromise between the increased workload and increased accuracy.

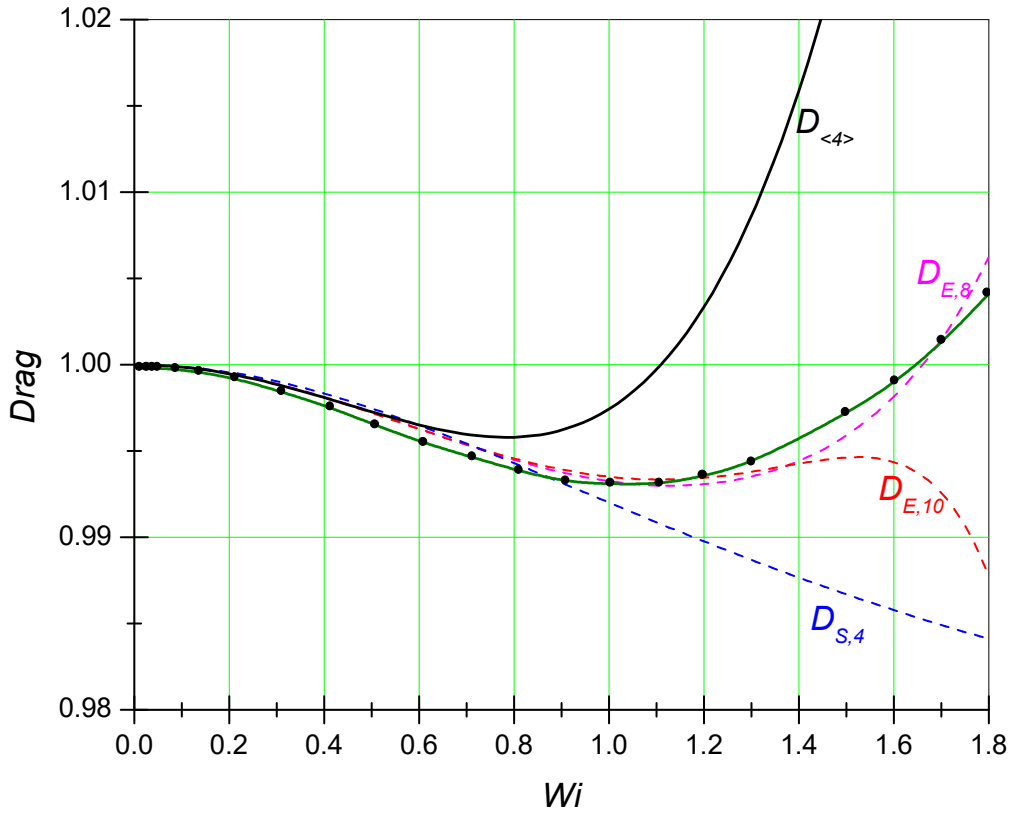

Figure (2.5): Normalized drag force for ***no-slip*** ($k = 0$) for the Oldroyd-B model ($\eta = 8/9$).
Black solid lines: perturbation results up to 4th order.
Line with symbols: numerical results by Bodart & Crochet [39] for the smallest sphere-to-cylinder ratio 0.02, normalized by the corresponding Newtonian value.
Upper dash lines: Euler's transformation up to 8th and 10th (see Eqs (2.36)-(2.37)).
Lowest dash line: accelerated results from Eq.(2.31)

2.5 RESULTS AND DISCUSSION

For comparison, we start the discussion with the no-slip case despite the fact that most of the results have been known from earlier work [17].

DRAG ON THE SPHERE: NO-SLIP ($k \to 0$)

When the slip coefficient goes to zero, namely for the standard no-slip condition on the particle, the following expression is derived for the UCM/Oldroyd-B models:

$$D_{\langle 4\rangle} = 1 - Wi^2\,\eta\left(\frac{258}{25025}+\frac{\eta}{175}\right) + Wi^4\,\eta\left(\begin{array}{c}\dfrac{2524971}{181060880}+\dfrac{117018471\,\eta}{681360680000}\\ -\dfrac{447910935363\,\eta^2}{181241940880000}+\dfrac{2426923127\,\eta^3}{4769524760000}\end{array}\right) \quad (2.39)$$

Eq.(2.39) fully agrees with that derived in Ref. [17] up to fourth order in Wi. One can easily see that the $O(Wi^2)$ term is negative while the $O(Wi^4)$ term is positive; the numerical values in the last parentheses are 0.01395, $0.0001717\,\eta$, $-0.002471\,\eta^2$ and $0.0005088\,\eta^3$. Results for the drag force as a function of the Weissenberg number are presented in Figures (2.6a,b) for the Oldroyd-B and exp-PTT models, respectively. The rheological parameter is $\varepsilon = 0.1$, while for all models the polymer viscosity ratio is $\eta = 0.9$. Both Eq.(2.39) (solid lines) and the corresponding expression derived from Eq.(2.31) (dots) are shown. The original series solution, Eq.(2.39), shows a decrease of the drag up to $Wi \sim 0.8 - 1.3$ (depending on the constitutive model) and then the drag starts to increase. It is interesting that this behavior has been confirmed experimentally [7] and numerically in Ref. [39] for the Oldroyd-model (see the previous section and Figure (2.5)).

However, when Eq.(2.39) is transformed according to Eq.(2.31) a monotonic variation of the drag force with Wi is predicted, i.e. the effect of viscoelasticity is that the drag monotonically decreases (or, equivalently, the translational velocity monotonically increases when the force on the particle is kept fixed). Also note, that this decrease is more substantial in the exp-PTT models. It is assumed that it is caused by the shear thinning and lower extensional thickening associated with these models and parameters used here. Our assertion is corroborated by the numerical simulations of Chilcott & Rallison [6], Yang & Khomami [40] and Castillo et al. [41] who also showed a decrease of the drag at small Weissenberg number. Therefore, it appears that our transformed fourth-order perturbation results agree with the available numerical results (see the previous discussion and Figure (2.5)). We emphasize though that the drag may increase at Weissenberg number larger than one, and more in experimental data than predicted by the numerical simulations [17] [41]. It is obvious that the disagreement between theory/simulations and experiments should be attributed to the inability of the utilized constitutive models to predict the correct response of highly viscoelastic fluids under flow deformation; the interested reader is also referred to the corresponding discussion in Ref. [41]. Perhaps other constitutive models should be used, such as that presented by Garduno et al. [42], although there are still issues that need careful consideration.

DRAG ON THE SPHERE: PERFECT SLIP $(k \to \infty)$

When the slip coefficient goes to infinity, perfect slip is imposed on the particle, and the following expression is derived for the UCM/Oldroyd-B models:

$$D_{\langle 4\rangle} = \frac{2}{3} + Wi^2\,\frac{2\,\eta}{25}\left(1-\frac{2\,\eta}{9}\right) + Wi^4\eta\left(\begin{array}{c}\dfrac{9}{49}-\dfrac{738877\,\eta}{5788125}\\ +\dfrac{12667304\,\eta^2}{445685625}+\dfrac{2812\,\eta^3}{17827425}\end{array}\right) \quad (2.40)$$

Note that the perfect slip case should be considered as an idealized state which cannot be encountered in real systems; it is useful only as a lower bound for the drag force on the particle. Eq.(2.40) shows that in contrast to the zero-slip case, both the $O(Wi^2)$ and $O(Wi^4)$ terms are strictly positive for $0 < \eta \leq 1$ and therefore the effect of viscoelasticity increases the drag force compared to its Newtonian value, i.e. the first term in Eq.(2.40). Notice also that the coefficients decrease in magnitude; for instance the numerical values in the $O(Wi^4)$ term are 0.1837, $0.1277\,\eta$, $0.02842\,\eta^2$ and $0.0001577\,\eta^3$. Based on these coefficients one can expect good convergence for any value of η ($0 < \eta \leq 1$). It is also expected that $D_{\langle 4 \rangle}$ is accurate up to $O(1)$ values of the Weissenberg number. Indeed, In Figure (2.7a), comparison against the convergence acceleration results, $D_{S,4}$, shows convergence up to $Wi \sim 0.4$ with a monotonic drag increase being even more pronounced in $D_{S,4}$ than $D_{\langle 4 \rangle}$. In fact, for the $D_{S,4}$ a singular point of the solution is predicted at $Wi_c \approx 0.834$. Given the relatively low values of the Weissenberg number ($Wi < 1$) and the discussion in Subsection "Accuracy of the solution" there is a high confidence for the validity and accuracy of these results. The substantial increase on the drag is caused by the fact that in the perfect-slip case the shear character of the flow on the sphere is eliminated allowing for the substantial extensional thickening characteristics (and the singularity in pure extensional flow) of the Oldroyd-B model to prevail. In contrast to the Oldroyd-B model, no singularity is predicted for the exp-PTT model which are shown in Figures (2.7b,c), respectively. This is consistent to the absence of singularity in pure extensional flow in these two models. It is also another indication that the UCM/Olrdoyd-B models may not be suitable for the problem under consideration. Moreover, an almost constant drag is predicted using the Shanks transformation, i.e. Eq.(27), for the exp-PTT model a very slight increase of the drag is observed. Therefore, it appears that the choice of the constitutive model is important. Finally, it is worth noting that there is a good agreement between the original perturbation results and their transformed values up to $Wi \sim 1$. For larger Wi the discrepancy becomes bigger, and the original series results eventually become a-physical.

DRAG ON THE SPHERE: FINITE SLIP ($k = 0.5$)

As mentioned above for the Newtonian fluid, the drag force D reduces from unity at $k = 0$, to $2/3$ as k goes to infinity; see Eq.(2.27). Between these two limiting cases, we chose $k = 0.5$ in order to show the effect of a finite dimensionless slip coefficient since for this value we already get an appreciable decrease of the drag, i.e. $D = 0.8$. For the UCM/Oldroyd-B models, and setting $k = 0.5$ in Eqs (2.28-2.30) we find:

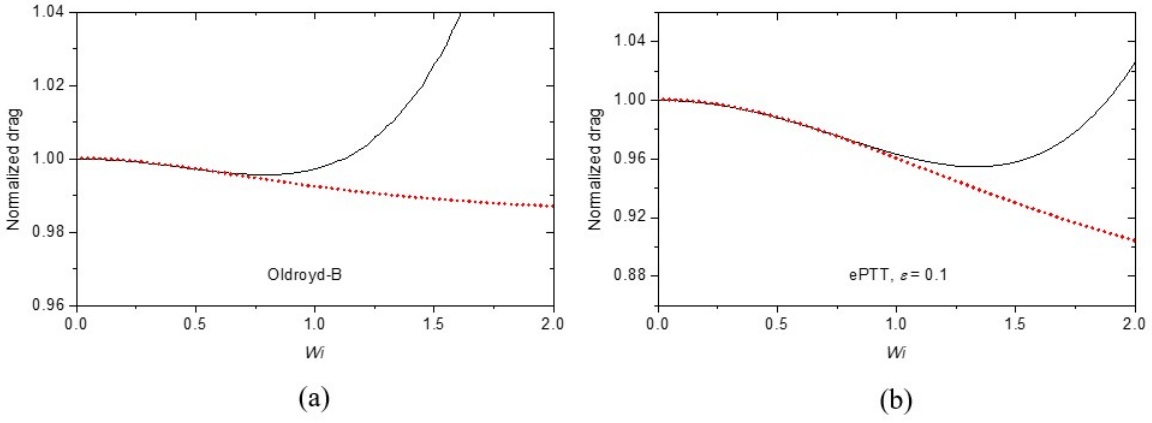

Figure (2.6): Normalized drag force for ***no-slip*** ($k = 0$). The polymer viscosity ratio is $\eta = 0.9$. Black solid lines: perturbation results up to $O(Wi^4)$; Red lines with dots: acceleration results

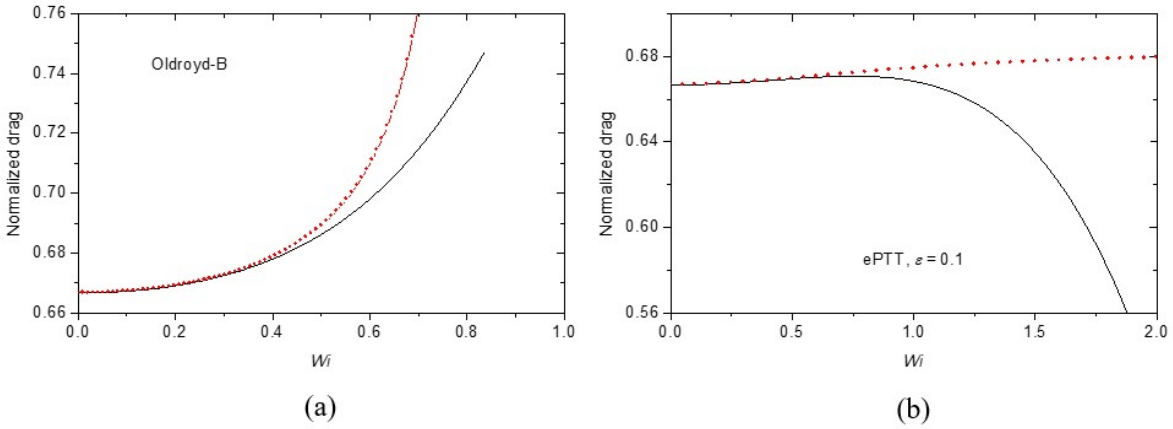

Figure (2.7): Normalized drag force for **perfect slip** ($k \to \infty$). The polymer viscosity ratio is $\eta = 0.9$. Black solid lines: perturbation results up to $O(Wi^4)$; Red lines with dots: acceleration results

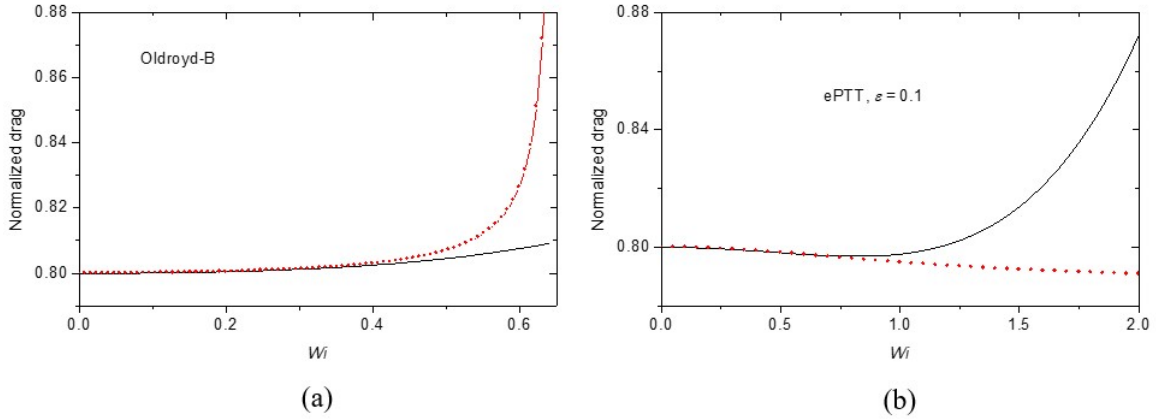

Figure (2.8):Normalized drag force for **finite slip** ($k = 0.5$). The polymer viscosity ratio is $\eta = 0.9$. Black solid lines: perturbation results up to $O(Wi^4)$; Red lines with dots: acceleration results

$$D_{\langle 4\rangle} = \frac{4}{5} + Wi^2\,\eta\left(\frac{217002}{15640625} - \frac{136\,\eta}{109375}\right) + Wi^4\eta\left(\begin{array}{c}\dfrac{7402399272}{176817265625} - \dfrac{29267959590143\,\eta}{5822173779296875} \\ -\dfrac{21810287859365101\,\eta^2}{1548698225292968750} + \dfrac{1107195765724\,\eta^3}{197308740234375}\end{array}\right) \tag{2.41}$$

The coefficients of the fourth-order term are 0.0418647, $-0.00502698\,\eta$, $-0.014083\,\eta^2$, and $0.00561149\,\eta^3$. One can verify that both coefficients of Wi^2 and Wi^4 are strictly positive for any value of the polymer viscosity ratio, clearly showing an increase of the total drag on the particle. The results from Eq.(2.41) and the transformed expression based on Eq.(2.31) are presented in Figure (2.8a). The corresponding results for the exp-PTT model are shown in Figures (2.8b,c), respectively. The rheological parameters η and ε are the same as in Figures (2.6)-(2.7). The results are qualitatively similar to those predicted for the perfect slip case albeit quantitively the relative drag with respect to the Newtonian value is smaller in partial slip than in perfect slip. This can be clearly seen with the exp-PTT model (compare Figures (2.8b,c) with Figures (2.7b,c)). Notice that

with the Oldroyd-B model, shown in Figure (2.8a), a singularity is predicted at a smaller Weissenberg number $Wi_c \approx 0.6518$ compared to the perfect slip case.

VELOCITY RESULTS

In Figure (2.9), we present the slip velocity $v_\theta(r=1,\theta)$ as a function of the polar angle θ, where $\theta = 0$ corresponds to the north pole of the sphere and $\theta = \pi$ to the south pole. As expected, due to the axisymmetry of the problem and the spherical coordinate system, the slip velocity at the poles is zero. It increases as we move away from the north pole, reaches a maximum and then decreases to zero at the south pole. Notice however, that the maximum is not always observed at the equator, i.e. at $\theta = \pi/2$, but mostly before or even after that, which shows that the symmetry with respect to the y-axis breaks. This is caused exclusively due to viscoelasticity, since the slip velocity for the Newtonian fluid is $v_{\theta,0}(r=1,\theta) = (3/2 - c_0)\sin(\theta)$ (see Eq.(2.13)). Figure (2.9) also shows clearly that the increase of the slip coefficient k enhances the magnitude of the fluid velocity on the surface of the particle. For a Newtonian fluid and perfect slip $c_0 \to 1$ and therefore $v_{\theta,0}(r=1,\theta) \to (1/2)\sin(\theta)$. As far as the effect of the Wi number is concerned, for small k is hardy observable. For a higher value of k, i.e. for $k = 0.5$, a slight increase of the slip velocity is seen at the upper part of the sphere, while at the lower part the slip velocity remains practically the same. For perfect slip, the effect of viscoelasticity is larger compared to the finite slip case, although the differences are located at the lower part of the sphere instead of the upper part.

The streamlines for a Newtonian ambient fluid ($Wi = 0$) with no-slip on the surface of the sphere are well-known and can be found elsewhere (see for instance in Ref. [17]). In order to focus on the effect of slip we present results for the normalized stream function $\Delta\Psi_n := (\Psi - \Psi_0)/Wi$. i.e. for the deviation from the Newtonian fluid scaled by the Weissenberg number. The $\Delta\Psi_n$ contours are shown in Figures (2.10a), b and c in increments of 0.02 for the no-slip, finite slip, and perfect slip cases, respectively. The symmetry with respect to the z-axis is clearly demonstrated. However, the symmetry with respect to the y-axis, observed for the Newtonian fluid, has been broken. It is interesting that for the no-slip case both positive and negative values of $\Delta\Psi_n$ are observed; the zero contour which marks the transition from positive to negative values is also seen. Note that as we move from the no-slip to the finite and perfect slip cases, the regions with positive values gradually shrink and disappear.

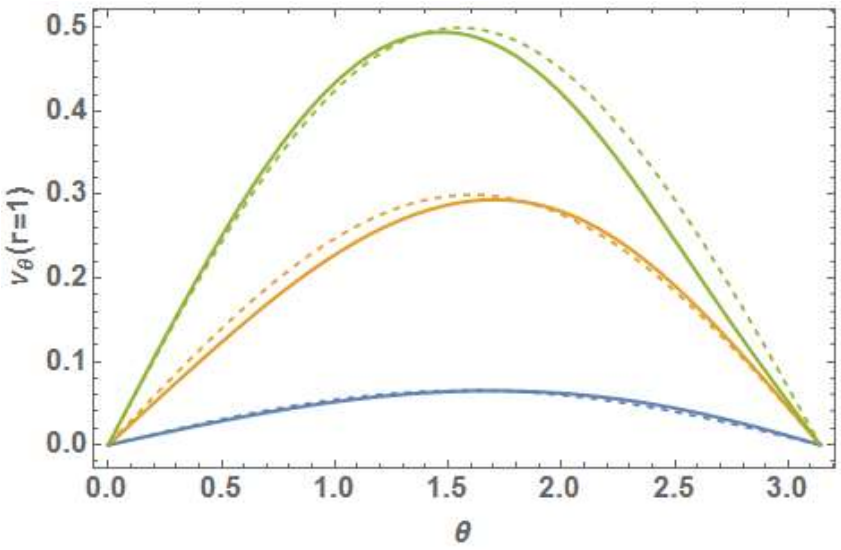

Figure (2.9): The slip velocity as function of the polar angle. Results are shown for the UCM model ($\eta = 1$, $\varepsilon = 0$). Solid lines: $Wi = 0.1$, Dashed lines: $Wi = 0.5$

In Figure (2.11), we present the contours for the axial velocity component $v_z = \mathbf{e_z} \cdot \mathbf{v}$ which far from the particle becomes constant, i.e. at $r \to \infty$, $v_z \to v_z^\infty = -1$. The parameters are the same parameters as in Figures (2.9)-(2.10). For a Newtonian fluid, a fully symmetric scenario with respect to both y and z axes is predicted because the axial velocity can be written in the form $v_{z,0} = \left(\hat{v}_{r,0} + \hat{v}_{\theta,0}\right)\cos^2(\theta) - \hat{v}_{\theta,0}$ where $\hat{v}_{r,0}$ and $\hat{v}_{\theta,0}$ are the radial parts of the zero-order velocity components (see Eq.(2.13)). However, when viscoelasticity is taken into account, the appearance of the higher cosine Fourier modes in the solution breaks the symmetry with respect to the y-axis. The no-slip case, shown in Figure (2.11a), produces closed contours which do not intersect with the surface of the sphere on which the axial velocity is zero. When slip is allowed, either finite (Figure (2.11b)) or perfect slip (Figure (2.11c)), the non-zero contours near the sphere cease to be closed but instead they start/end on the sphere. It also appears that the magnitude of the contours is larger compared to the no-slip case which, again, is because slippage is allowed on the surface of the particle.

CONFORMATION RESULTS

Finally, in Figure (2.12), we present the contours for $\mathrm{tr}(\mathbf{c})$; the latter corresponds to the extension of the polymer molecules due to flow. Recall also that for a Newtonian fluid, or for no-flow, $\mathbf{c} = \mathbf{I}$ and thus $\mathrm{tr}(\mathbf{c}) = 3$. The parameter values are the same as in Figure (2.8). Symmetry with respect to vertical axis is observed in all cases, while the symmetry with respect to the horizontal axis breaks due to viscoelasticity. For the no-slip condition the largest extension of the polymer molecules is observed close to the equator ($\theta = \pm\pi/2$) as well as below the sphere. As expected, the extension is enhanced as the dimensionless slip coefficient k increases. We also see that as k increases more complicated structures become apparent close to the surface of the sphere; obviously the full resolution of the flow field close to the particle is more demanding that the no-slip case.

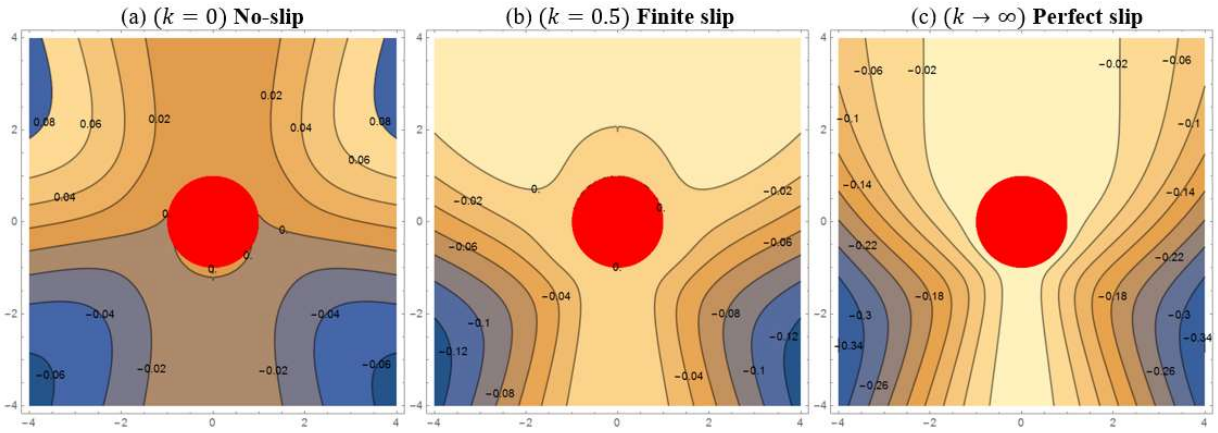

Figure (2.10): Contours for the normalized stream function $\Delta\Psi_n := \left(\Psi - \Psi_0\right)/Wi$
Results are shown for the UCM model ($\eta = 1, \varepsilon = 0$) with $Wi = 0.8$

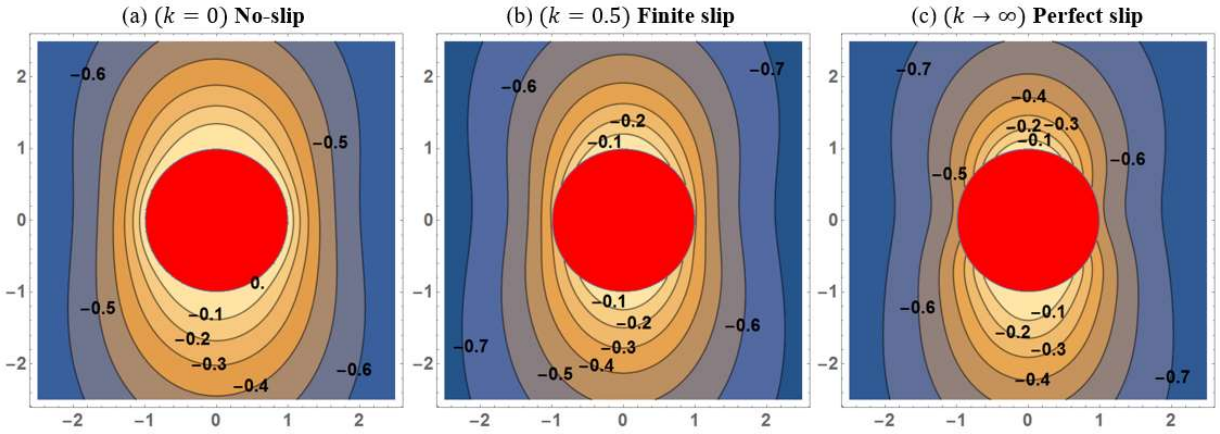

Figure (2.11): v_z contours for the UCM fluid with $Wi = 0.8$ ($\eta = 1, \varepsilon = 0$)

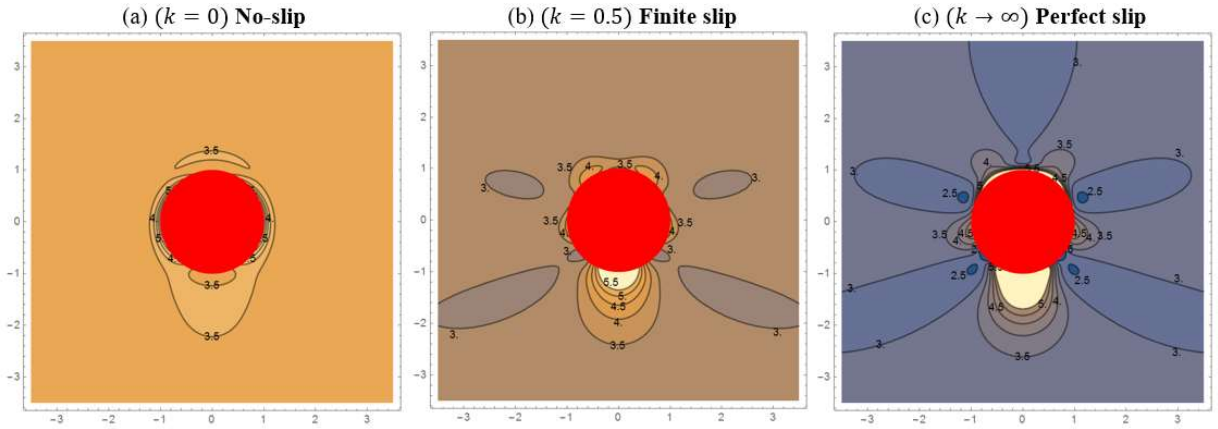

Figure (2.12): $\mathrm{tr}(\mathbf{c})$ contours for a UCM fluid ($\eta = 1, \varepsilon = 0$) with $Wi = 0.8$

2.6 CONCLUSIONS

We have investigated analytically, by deriving fourth-order perturbation solutions, the steady translation of a spherical particle in a viscoelastic fluid assuming Navier-type linear slip on the surface of the particle. Our solutions for the drag force have also been processed with techniques that accelerate the convergence of series in order to increase the accuracy and extend the domain of convergence of the original perturbation solutions.

In the limit of Newtonian matrix fluids, we have confirmed the known analytical results that reveal the decrease of the drag force on the particle with increasing slip. However, for the viscoelastic cases the results are more complicated and depend on the choice of the constitutive model. The analytical results have been carefully checked for their correctness and have been validated for accuracy in the limit of no-slip against numerical results from the literature. The analysis has shown consistently that the techniques that accelerate the convergence of series extend reliably the accuracy of the total drag force on the particle up to $Wi \sim 1$.

For the Oldroyd-B model, and under perfect slip conditions on the particle, both the original perturbation series and the convergence acceleration solutions have shown a dramatic increase of the drag force as the Weissenberg number increases. Furthermore, the convergence acceleration results for this model indicate a singular point of the solution at a finite, order one, Weissenberg number; however, it is not possible to be definitive on this point using only relatively low (fourth order here) perturbation approximations and one should only use this feature simply as indicative of the presence of a significant drag enhancement with this model. In contrast to the Oldroyd-B model, a singularity is not predicted for the exp-PTT model. For all models, we have shown that viscoelasticity increases the dimensionless drag, normalized with respect to the corresponding Newtonian result, monotonically with increasing the slip coefficient. This is attributed to the dominating role of the extensional thickening properties of the models as the intensity of shearing close to the particle diminishes.

The slip velocity on the surface of the sphere increases as the slip coefficient increases, whereas the effect of viscoelasticity appears to be minor. Finally, we have shown that viscoelasticity destroys some of the symmetries of the flow field around the sphere which are observed for a Newtonian fluid, as well as that complicated flow structures close to the particle and especially in the wake, are developed. Those structures require special numerical techniques in order to be resolved accurately.

APPENDIX A

We give here the analytical solutions which are not given in the main text, namely $\mathbf{v}_2, p_2$, for the exp-PTT, model. We also provide the non-trivial components of the viscoelastic extra-stress tensor $\boldsymbol{\tau}$, up to 2nd-order, which according to the perturbation scheme are $\tau_{ij} \approx \dot{\gamma}_{ij,0} - \sigma_{ij,0} Wi + \left(\dot{\gamma}_{ij,2} - \sigma_{ij,1}\right) Wi^2$ where $i = r, \theta$ and $j = r, \theta$.

UCM/OLDROYD-B MODEL

$$-\sigma_{rr,0} = \left(4 + \frac{12}{r^8} - \frac{24}{r^6} + \frac{16}{r^4} - \frac{8}{r^2}\right) + \left(\frac{32}{r^6} - \frac{64}{r^4} + \frac{32}{r^2}\right)\cos(4\theta)$$

$$-\sigma_{rr,1} = \left\{\begin{array}{c}\left(8+\frac{24}{r^{12}}-\frac{144}{r^{10}}+\frac{296}{r^{8}}-\frac{272}{r^{6}}+\frac{120}{r^{4}}-\frac{32}{r^{2}}\right)\cos(2\theta)\\ +\left(-\frac{144}{r^{8}}+\frac{432}{r^{6}}-\frac{432}{r^{4}}+\frac{144}{r^{2}}\right)\cos(6\theta)\end{array}\right\}$$

$$-\sigma_{r\theta,0} = \left(\frac{32}{r^{6}}-\frac{40}{r^{4}}+\frac{8}{r^{2}}\right)\sin(4\theta)$$

$$-\sigma_{r\theta,1} = \left\{\begin{array}{c}\left(-8-\frac{168}{r^{12}}+\frac{672}{r^{10}}-\frac{904}{r^{8}}+\frac{440}{r^{6}}-\frac{24}{r^{4}}-\frac{8}{r^{2}}\right)\sin(2\theta)\\ +\left(-\frac{144}{r^{8}}+\frac{312}{r^{6}}-\frac{192}{r^{4}}+\frac{24}{r^{2}}\right)\sin(6\theta)\end{array}\right\}$$

$$-\sigma_{r\theta,0} = \left(\frac{32}{r^{6}}-\frac{40}{r^{4}}+\frac{8}{r^{2}}\right)\sin(4\theta)$$

$$-\sigma_{r\theta,1} = \left\{\begin{array}{c}\left(-8-\frac{168}{r^{12}}+\frac{672}{r^{10}}-\frac{904}{r^{8}}+\frac{440}{r^{6}}-\frac{24}{r^{4}}-\frac{8}{r^{2}}\right)\sin(2\theta)\\ +\left(-\frac{144}{r^{8}}+\frac{312}{r^{6}}-\frac{192}{r^{4}}+\frac{24}{r^{2}}\right)\sin(6\theta)\end{array}\right\}$$

$$-\sigma_{\theta\theta,0} = \left(4+\frac{60}{r^{8}}-\frac{72}{r^{6}}+\frac{16}{r^{4}}+\frac{8}{r^{2}}\right)+\left(-\frac{32}{r^{6}}+\frac{16}{r^{4}}\right)\cos(4\theta)$$

$$-\sigma_{\theta\theta,1} = \left\{\begin{array}{c}\left(-8+\frac{840}{r^{12}}-\frac{2448}{r^{10}}+\frac{2200}{r^{8}}-\frac{544}{r^{6}}-\frac{24}{r^{4}}-\frac{16}{r^{2}}\right)\cos(2\theta)\\ +\left(\frac{144}{r^{8}}-\frac{192}{r^{6}}+\frac{48}{r^{4}}\right)\cos(6\theta)\end{array}\right\}$$

EXP-PTT MODEL

Likewise, the solution for the exp-PTT model is given with the aid of Eq.(1.14) and using the superscript "*P*":

$$p_2^P = p_2 + \varepsilon\,\eta\left\{\begin{array}{c}\left(\frac{1728}{7r^{12}}-\frac{432}{r^{10}}-\frac{768}{5r^{8}}+\frac{544}{r^{6}}-\frac{256}{r^{4}}+\frac{10256}{105r^{2}}\right)\cos(2\theta)\\ +\left(\frac{128}{r^{6}}-\frac{832}{5r^{4}}+\frac{48}{r^{2}}\right)\cos(6\theta)\end{array}\right\}$$

$$v_{r,2}^P = v_{r,2} + \varepsilon\,\eta\left\{\begin{array}{c}\left(\frac{36}{7r^{11}}-\frac{72}{5r^{9}}+\frac{192}{5r^{7}}-\frac{304}{3r^{5}}+\frac{5812}{105r^{3}}+\frac{1768}{105r}-\frac{128\ln(r)}{r^{3}}\right)\cos(2\theta)\\ +\left(-\frac{124}{5r^{7}}+\frac{288}{5r^{5}}-\frac{204}{5r^{3}}+\frac{8}{r}\right)\cos(6\theta)\end{array}\right\}$$

$$v_{\theta,2}^P = v_{\theta,2} + \varepsilon\,\eta\left\{\begin{array}{c}\left(\frac{180}{7r^{11}}-\frac{288}{5r^{9}}+\frac{576}{5r^{7}}-\frac{608}{3r^{5}}+\frac{12532}{105r^{3}}-\frac{128\ln(r)}{r^{3}}\right)\sin(2\theta)\\ +\left(-\frac{124}{5r^{7}}+\frac{192}{5r^{5}}-\frac{68}{5r^{3}}\right)\sin(6\theta)\end{array}\right\}$$

$$\sigma^P_{rr,0} = \sigma_{rr,0}, \quad \sigma^P_{r\theta,0} = \sigma_{r\theta,0}, \quad \sigma^P_{\theta\theta,0} = \sigma_{\theta\theta,0}$$

$$-\sigma^P_{rr,1} = -\sigma_{rr,1} + \varepsilon \left\{ \begin{array}{c} \left(-16 + \frac{432}{r^{12}} - \frac{864}{r^{10}} + \frac{288}{r^8} + \frac{256}{r^6} - \frac{32}{r^4} - \frac{64}{r^2}\right)\cos(2\theta) \\ + \left(-\frac{144}{r^8} + \frac{192}{r^6} - \frac{16}{r^4} - \frac{32}{r^2}\right)\cos(6\theta) \end{array} \right\}$$

$$-\sigma^P_{r\theta,1} = -\sigma_{r\theta,1} + \varepsilon \left\{ \begin{array}{c} \left(16 + \frac{432}{r^{12}} - \frac{864}{r^{10}} + \frac{864}{r^8} - \frac{512}{r^6} + \frac{224}{r^4} - \frac{64}{r^2}\right)\sin(2\theta) \\ + \left(-\frac{144}{r^8} + \frac{192}{r^6} - \frac{112}{r^4} + \frac{32}{r^2}\right)\sin(6\theta) \end{array} \right\}$$

$$-\sigma^P_{\theta\theta,1} = -\sigma_{\theta\theta,1} + \varepsilon \left\{ \begin{array}{c} \left(16 - \frac{432}{r^{12}} + \frac{864}{r^{10}} - \frac{288}{r^8} - \frac{256}{r^6} + \frac{32}{r^4} + \frac{64}{r^2}\right)\cos(2\theta) \\ + \left(\frac{144}{r^8} - \frac{192}{r^6} + \frac{16}{r^4} + \frac{32}{r^2}\right)\cos(6\theta) \end{array} \right\}$$

APPENDIX B

CONSTANTS FOR THE 2ND ORDER VELOCITY PROFILE

The coefficients which appear in Eq.(2.18a) are:

$$f_{1,3} = \left(\frac{7151}{50050} + \frac{8\eta}{525}\right)c_0^3 - \left(\frac{7681}{10010} + \frac{4\eta}{105}\right)c_0^2 + \left(\frac{503}{1430} + \frac{13\eta}{10}\right)c_0 + \frac{11\eta}{30}c_1 - c_2 + \frac{3}{50}c_3 - \frac{567}{715}$$

$$f_{1,4} = \left(2\eta - \frac{11}{8}\right)c_0^2 + \frac{\eta c_0 c_1}{3}$$

$$f_{1,5} = \left\{\begin{array}{c} -\left(\frac{74727}{100100} + \frac{14221\eta}{50050}\right)c_0^3 + \left(\frac{1317}{220} - \frac{30509\eta}{5720}\right)c_0^2 + \left(-\frac{7461}{2860} + \frac{9099\eta}{5720}\right)c_0 \\ -\frac{3\eta}{4}\left(\frac{1}{10} + c_0\right)c_1 - \frac{3c_3}{50} - \frac{99}{520} \end{array}\right\}$$

$$f_{1,6} = \frac{3\eta}{4}c_0^3 + \left(-\frac{19}{4} + \frac{23\eta}{8}\right)c_0^2 + \left(\frac{19}{4} - \frac{23\eta}{8}\right)c_0 - \frac{\eta}{12}\left(\frac{7}{2} - 5c_0\right)c_1$$

$$f_{1,7} = c_0^2\left(\frac{87}{77} - \frac{215\eta}{462}\right)(c_0 - 1)$$

$$f_{1,8} = \frac{9}{8}(c_0 - 1)^2$$

$$f_{1,9} = -\left(\frac{191}{286} + \frac{9\eta}{572}\right)(c_0^3 - 2c_0^2 + c_0)$$

where the constants c_2 and c_3 are:

$$c_2 = 3\left\{\begin{array}{c} -180180k^5(2\eta - 9) + 10296k^4(109 + 9\eta) \\ +286k^3(268\eta - 87) - 273k^2(258 + 143\eta) \\ -36k(258 + 143\eta) - 2(258 + 143\eta) \end{array}\right\} \times \left(100100(1 + 3k)^4(1 + 5k)\right)^{-1}$$

$$c_3 = 15\left\{\begin{array}{c} 61776k^5(890 + 113\eta) \\ +572k^4(123159 + 10046\eta) \\ -26k^3(-1581144 + 65123\eta) \\ +3k^2(3818322 + 269273\eta) \\ +40k(37407 + 4535\eta) \\ +2(37407 + 4535\eta) \end{array}\right\} \times \left(32032(1 + 3k)^3(1 + 5k)(1 + 7k)\right)^{-1}$$

The coefficients which appear in Eq. (2.18b) are:

$$f_{3,3} = \frac{3}{2}(\eta - 1)c_0 + \frac{\eta c_1}{2} + \frac{c_3}{10}$$

$$f_{3,4} = \left(-\frac{21}{8} + 4\eta\right)c_0^2 + \frac{2}{3}\eta c_0 c_1$$

$$f_{3,5} = \left\{\begin{matrix} -\left(\frac{679}{572} + \frac{439\eta}{858}\right)c_0^3 + \left(\frac{439}{44} - \frac{30509\eta}{3432}\right)c_0^2 + \left(-\frac{2487}{572} + \frac{3033\eta}{1144}\right)c_0 \\ -\frac{\eta}{4}\left(5c_0 + \frac{1}{2}\right)c_1 - \frac{c_3}{10} - \frac{33}{104} \end{matrix}\right\}$$

$$f_{3,6} = \frac{5\eta c_0^3}{4} + \left(-\frac{27}{4} + \frac{33\eta}{8}\right)(c_0^2 - c_0) + \frac{\eta}{4}\left(\frac{7c_0}{3} - \frac{3}{2}\right)c_1$$

$$f_{3,7} = \left(\frac{16}{11} - \frac{47\eta}{66}\right)(c_0^3 - c_0^2)$$

$$f_{3,8} = \frac{3}{8}(c_0 - 1)^2$$

$$f_{3,9} = -\left(\frac{93}{286} + \frac{15\eta}{572}\right)(c_0^3 - 2c_0^2 + c_0)$$

The coefficients which appear in Eq.(2.18c) are:

$$g_{1,5} = \frac{1}{2}\left(17\eta - \frac{51}{2}\right)c_0^2 + \frac{17}{6}\eta c_0 c_1$$

$$g_{1,6} = \frac{1}{7}(48 + 59\eta)c_0^3$$

$$g_{1,7} = \left(\frac{135}{2} - 18\eta\right)(c_0^2 - c_0) - 18\eta c_0^3 + 3\eta(2 - 3c_0)c_1$$

$$g_{1,8} = -\frac{17}{132}(393 + 107\eta)(c_0 - 1)c_0^2$$

$$g_{1,9} = \frac{19}{4}(c_0 - 1)(27 + 3c_0(4\eta c_0 - 9) + 2\eta c_1)$$

$$g_{1,10} = \frac{27}{286}(1285 - 352\eta)(c_0 - 1)^2 c_0$$

The coefficients which appear in Eq. (2.18d) are:

$$g_{3,5} = \frac{5}{4}c_0\left((6\eta - 9)c_0 + 2\eta c_1\right)$$

$$g_{3,6} = \left(4 + \frac{17\eta}{3}\right)c_0^3$$

$$g_{3,7} = -10\eta c_0^3 + \left(\frac{63}{2} - 6\eta\right)(c_0^2 - c_0) + \eta\left(2 - \frac{11c_0}{3}\right)c_1$$

$$g_{3,8} = \frac{3}{44}(279 + 37\eta)(1 - c_0)c_0^2$$

$$g_{3,9} = \frac{5}{4}(c_0 - 1)(27 + 3c_0(4\eta c_0 - 9) + 2\eta c_1)$$

$$g_{3,10} = \frac{3}{26}(249 - 64\eta)(c_0 - 1)^2 c_0$$

The constants $d_{4,1}$, $d_{4,2}$, $d_{4,3}$ and $d_{4,4}$ that appear in Eq. (2.32) are:

$$d_{4,1} = \begin{Bmatrix} 0.0139454 + 0.292854\,k + 2.72467\,k^2 + 14.7506\,k^3 \\ +52.7676\,k^4 + 68.6521\,k^5 + 133.898\,k^6 \end{Bmatrix}$$

$$d_{4,2} = \begin{Bmatrix} 0.000171742 + 0.00618272\,k + 0.0857293\,k^2 - 0.444484\,k^3 - 2.55957\,k^4 \\ -44.1639\,k^5 - 478.207\,k^6 - 1091.79\,k^7 - 2986.88\,k^8 - 9771.27\,k^9 \end{Bmatrix}$$

$$d_{4,3} = \begin{Bmatrix} -0.00247134 - 0.101325\,k - 1.95022\,k^2 - 25.0706\,k^3 - 208.481\,k^4 - 1295.25\,k^5 \\ -6198.88\,k^6 - 20415.3\,k^7 - 34941.2\,k^8 - 17629.1\,k^9 + 10877.8\,k^{10} \end{Bmatrix}$$

$$d_{4,4} = \begin{Bmatrix} 0.00050884 + 0.0234066\,k + 0.553651\,k^2 + 8.53058\,k^3 \\ +91.8112\,k^4 + 541.02\,k^5 + 2425.11\,k^6 + 14656.1\,k^7 \\ +62770.7\,k^8 + 105735.\,k^9 + 33477.1\,k^{10} + 301.845\,k^{11} \end{Bmatrix}$$

TOTAL DRAG FORCE: EXP-PTT MODEL

For the 2nd order correction, we find:

$$\begin{aligned} D_2 &= D_2^{OLD} \\ &+ \begin{Bmatrix} \eta \dfrac{3\left(-86 - 3454\varepsilon + 13k\left(-2(43 + 572\varepsilon) + 11k\left(-43 - 572\varepsilon + 6k(31 + 63k - 54(4 + 7k)\varepsilon)\right)\right)\right)}{25025(1 + 3k)^4} \\ -\eta^2 \dfrac{(1 + 2k)\left(2 + k\left(32 + k\left(209 + 18k(-53 + 70k)\right)\right)\right)}{350(1 + 3k)^4(1 + 5k)} \end{Bmatrix} \end{aligned}$$

where theD_2^{OLD} is given by Eq.(2.28). For the 4th order correction, we find:

$$D_4 = D_4^{OLD} + \eta\varepsilon \left(\begin{array}{c} \dfrac{\sum_{k=0}^{2} \varepsilon^k d_{4,1,k}}{(1 + 3k)^6} + \dfrac{\eta \sum_{k=0}^{2} \varepsilon^k d_{4,2,k}}{(1 + 3k)^7(1 + 5k)(1 + 7k)} \\ + \dfrac{\eta^2\left(d_{4,3,0} + \varepsilon d_{4,3,1}\right)}{(1 + 3k)^7(1 + 5k)^2(1 + 7k)} + \dfrac{\eta^3 d_{4,4,0}}{(1 + 3k)^7(1 + 5k)^3(1 + 7k)} \end{array} \right)$$

where D_4^{OLD} is given by Eq.(2.29) and the constants are:

$$d_{4,1,0} = \begin{Bmatrix} 0.0139454 + 0.292854k + 2.72467k^2 + 14.7506k^3 \\ +52.7676k^4 + 68.6521k^5 + 133.898k^6 \end{Bmatrix}$$

$$d_{4,1,1} = \begin{Bmatrix} -0.0424674 - 0.891814k - 5.49455k^2 - 89.5178k^3 \\ -322.592k^4 - 772.479k^5 - 1465.27k^6 \end{Bmatrix}$$

$$d_{4,1,2} = \begin{Bmatrix} 1.85156 + 4.16851k + 39.6008k^2 + 154.976k^3 \\ +581.161k^4 + 1136.1k^5 + 2082.86k^6 \end{Bmatrix}$$

$$d_{4,2,0} = \begin{Bmatrix} 0.0139454 + 0.502035k + 8.10761k^2 + 77.8776k^3 + 498.228k^4 \\ +2193.55k^5 + 6458.99k^6 + 12423.4k^7 + 16715.2k^8 + 14059.3k^9 \end{Bmatrix}$$

$$d_{4,2,1} = \begin{Bmatrix} -0.0424674 - 1.52882k - 21.8869k^2 - 239.714k^3 - 2149.11k^4 \\ -12544.1k^5 - 45355.9k^6 - 110697.k^7 - 185145.k^8 - 153854k^9 \end{Bmatrix}$$

$$d_{4,2,2} = \begin{Bmatrix} 1.85156 + 31.9419k + 233.589k^2 + 1239.37k^3 + 6155.16k^4 \\ +25014.9k^5 + 76659.3k^6 + 172928.k^7 + 267174k^8 + 218700k^9 \end{Bmatrix}$$

$$d_{4,3,0} = \begin{Bmatrix} -0.00247134 - 0.101325k - 1.95022k^2 - 25.0706k^3 - 208.481k^4 - 1295.25k^5 \\ -6198.88k^6 - 20415.3k^7 - 34941.2k^8 - 17629.1k^9 + 10877.8k^{10} \end{Bmatrix}$$

$$d_{4,3,1} = \begin{Bmatrix} -0.0156763 - 0.703992k - 16.5691k^2 - 238.851k^3 - 1683.77k^4 - 6196.79k^5 \\ -15541.5k^6 - 35568.6k^7 - 16255.9k^8 + 48936.7k^9 - 79955k^{10} \end{Bmatrix}$$

$$d_{4,4,0} = \begin{Bmatrix} 0.00050884 + 0.0234066k + 0.553651k^2 + 8.53058k^3 \\ +91.8112k^4 + 541.02k^5 + 2425.11k^6 + 14656.1k^7 \\ +62770.7k^8 + 105735k^9 + 33477.1k^{10} + 301.845k^{11} \end{Bmatrix}$$

BIBLIOGRAPHY

[1] E. A. Gryparis, S. D. Gkormpatsis, K. D. Housiadas and R. I. Tanner, "Viscoelastic planar elongational flow past an infinitely long cylinder," *Physics of Fluids,* vol. 31, no. 3, p. 033104, 2019.

[2] S. D. Gkormpatsis, E. A. Gryparis, K. D. Housiadas and A. N. Beris, "Steady sphere translation in a viscoelastic fluid with slip on the surface of the sphere," *Journal of Non-Newtonian Fluid Mechanics,* vol. 275, p. 104217, 2020.

[3] R. I. Tanner, "Review Article: Aspects of non-colloidal suspension rheology," *Physics of Fluids,* vol. 30, no. 10, (2018).

[4] L. G. Leal, Advanced Transport Phenomena, Cambridge: Cambridge University Press, 2007.

[5] L. G. Leal, "The motion of small particles in non-Newtonian fluids," *Journal of Non-Newtonian Fluid Mechanics,* vol. 5, pp. 33-78, (1979).

[6] M. D. Chilcott and J. M. Rallison, "Creeping flow of dilute polymer solutions past cylinders and spheres," *Journal of Non-Newtonian Fluid Mechanics,* vol. 29, pp. 381-432, (1988).

[7] R. G. Owens and T. N. Phillips, Computationally Rheology, London: Imperial College Press, (2002).

[8] K. D. Housiadas and R. I. Tanner, "Viscoelastic shear flow past an infinitely long and freely rotating cylinder," *Physics of Fluids,* vol. 30, no. 7, (2018).

[9] W. R. Hwang and M. A. Hulsen, "Direct numerical simulations of hard sphere particle suspensions in planar elongational flow," *Journal of Non-Newtonian Fluid Mechanics,* vol. 136, no. 2-3, pp. 167-178, (2006).

[10] M. V. Dyke, Perturbation Methods in Fluid Mechanics, Stanford,: The Parabolic Press, (1964).

[11] R. B. Bird, R. C. Armstrong and O. Hassanger, Dynamics of Polymeric Liquids, 2nd ed., vol. 1, New York: Wiley, (1987).

[12] Wolfram Research, Inc, Mathematica, 11.0 ed., Champaign, Illinois, (2017).

[13] M. A. Hulsen, "A sufficient condition for the positive definite configuration tensor in differential models," *Journal of Non-Newtonian Fluid Mechanics,* vol. 38, no. 1, pp. 93-100, (1990).

[14] G. G. Stokes, "On the Effect of the Internal Friction of Fluids on the Motion of Pendulums," *Cambridge Philos. Trans,* vol. 9, pp. 8-106, 1850.

[15] O. Hassanger, R. C. Armstrong and R. B. Bird, "Limitation on the use of the retarded motion expansion," *Journal of Non-Newtonian Fluid Mechanics,* vol. 34, no. 2, pp. 241-245, 1990.

[16] F. M. Leslie, "The slow flow of a viscoelastic liquid past a sphere," *The Quarterly Journal of Mechanics and Applied Mathematics,* vol. 14, no. 1, pp. 36-48, 1961.

[17] K. D. Housiadas and R. I. Tanner, "A high-order perturbation solution for the steady sedimentation of a sphere in a viscoelastic fluid," *Journal of Non-Newtonian Fluid Mechanics,* vol. 233, pp. 166-180, 2016.

[18] M. D. Allen and O. G. Raabe, "Slip correction measurements of spherical solid aerosol particles in an improved millikan apparatus," *Aerosol. Sci. Tech. ,* vol. 4, no. 3, pp. 269-286, 1985.

[19] J. P. Rothstein, "Slip on Superhydrophobic Surfaces," *Annual Review of Fluid Mechanics,* vol. 42, pp. 89-109, 2010.

[20] H. Müller-Mohnssen, D. Weiss and A. Tippe, "Concentration dependent changes of apparent slip in polymer solution flow," *Journal of Rheology,* vol. 34, no. 2, pp. 233-244, 1990.

[21] V. Mavrantzas and A. N. Beris, " Theoretical study of wall effects on the rheology of dilute polymer solutions," *Journal of Rheology,* vol. 36, no. 1, pp. 175-213, 1992.

[22] A. N. Beris and B. J. Edwards, Thermodynamics of Flowing Systems with Internal Microstructure, New York: Oxford Univ. Press, 1994.

[23] S. G. Hatzikiriakos, "Wall slip of molten polymers," *Progress in Polymer Science,* vol. 37, no. 4, pp. 624-643, 2012.

[24] S. G. Hatzikiriakos, "Slip mechanisms in complex fluid flows," *Soft Matter,* vol. 11, pp. 7851-7856, 2015.

[25] A. Y. Malkin and S. A. Patlazhan, "Wall slip for complex liquids – Phenomenon and its causes," *Advances in Colloid and Interface Science,* vol. 257, pp. 42-57, 2018.

[26] C. L. M. H. Navier, "Mémoire sur les lois du mouvement des fluides," *Mémoires de l'Académie (royale) des Sciences de l'Institut (imperial) de France,* vol. 6, pp. 389-440, 1827.

[27] A. B. Basset, A Treatise on Hydrodynamics, 2nd vol., Cambridge: Cambridge Univ. Press, 1888.

[28] N. Phan-Thien, "A nonlinear network viscoelastic model," *Journal of Rheology,* vol. 22, pp. 259-283, 1978.

[29] M. M. Denn, "Extrusion instabilities and wall slip," *Annual Review of Fluid Mechanics,* vol. 33, pp. 265-287, 2001.

[30] P. Panaseti, Viscoplastic flows with wall slip and pressure-dependent rheological parameters, University of Cyprus: Ph.D. thesis, 2018.

[31] A. Premlata and H. H. Wei, "The Basset problem with dynamic slip: slip-induced memory effect and slip-stick transition," *Journal of Fluid Mechanics,* vol. 886, pp. 431-449, 2019.

[32] J. S. Hadmard, "Mouvement permanent lent d' une sphere liquide et visqueuse dans un liquide visqueux," *Comptes Rendus de l' Academie des Sciences (París),* vol. 152, pp. 1735-1738, 1911.

[33] W. Rybczynski, "On the translator motion of a fluid sphere in a viscous medium," *Bulletin of the Polish Academy of Sciences Krakow,* pp. 40-46, 1911.

[34] C. T. Crowe and E. E. Michaelides, "Basic concepts and definitions, Taylor & Francis," in *Multiphase flow handbook, edited by Clayton T. Crowe*, Taylor & Francis, 2006, pp. 1.1-1.79.

[35] J. Happel and H. Brenner, Low Reynolds number hydrodynamics, New Jersey: Prentice-Hall Englewood Cliffs, 1965.

[36] D. Shanks, "Non-linear transformations of divergent and slowly convergent sequences," *Journal of Mathematics and Physics,* vol. 34, no. 1-4, pp. 1-42, 1955.

[37] K. D. Housiadas, "Improved convergence based on linear and non-linear transformations at low and high Weissenberg asymptotic analysis," *Journal of Non-Newtonian Fluid Mechanics,* vol. 247, pp. 1-14, 2017.

[38] K. D. Housiadas, "Steady sedimentation of a spherical particle under constant rotation," *Physial Review Fluids,* vol. 4, p. 103301, 2019.

[39] C. Bodart and M. J. Crochet, "The time-dependent flow of a viscoelastic fluid around a sphere," *Journal of Non-Newtonian Fluid Mechanics,* vol. 54, pp. 303-329, 1994.

[40] B. Yang and B. Khomami, "Simulations of sedimentation of a sphere in a viscoelastic fluid using molecular based constitutive models," *Journal of Non-Newtonian Fluid Mechanics,* vol. 82, no. 2-3, pp. 429-452, 1999.

[41] A. Castillo, W. L. Murch, J. Einarson, B. Mena, E. Shaqfeh and R. Zenit, "Drag coefficient for a sedimenting and rotating sphere in a viscoelastic fluid," *Physical Reviw Fluids,* vol. 4, p. 063302, 2019.

[42] I. E. Garduño, H. R. Tamaddon-Jahromi and M. F. Webster, "The falling sphere problem and capturing enhanced drag with Boger fluids," *Journal of Non-Newtonian Fluid Mechanics,* vol. 231, pp. 26-48, 2016.

[43] D. K. Hutchins, M. H. Harper and R. L. Felder, "Slip Correction Measurements for Solid Spherical Particles by Modulated Dynamic Light Scattering," *Aerosol Science and Technology,* vol. 22, no. 2, pp. 202-218, 1995.

[44] S. Gogte, P. Vorobieff, R. Truesdell and A. Mammoli, "Effective slip on textured superhydrophobic surfaces," *Physics of Fluids,* vol. 17, no. 5, 2005.

[45] H. J. Keh and S. H. Chen, "The Motion of a Slip Spherical Particle in an Arbitrary Stokes Flow," *European Journal of Mechanics - B/Fluids,* vol. 15, 1996.

[46] S. Senchenko and H. J. Keh, "Slipping Stokes flow around a slightly deformed sphere," *Physics of Fluids,* vol. 18, no. 8, 2006.